SiD Answers to IDAG Questions

12 June 2009

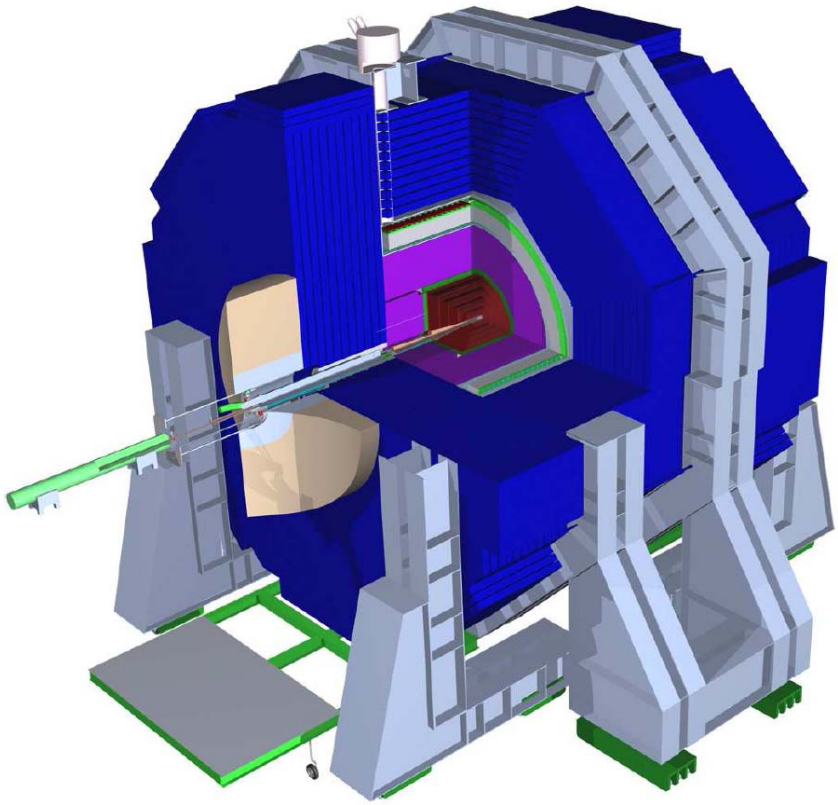

SiD Answers to IDAG Questions

SiD Answers to IDAG Questions **2**

I. Introduction **1**

A. What this document is 1
B. The IDAG questions 1
C. Organization of this document 3

II. Answers to Questions about Calorimeter Calibration **4**

A. The questions from IDAG *4*

B. EMCal Response *4*

Q2:What level of precision is required? *4*

Q2:How is it obtained? *4*

Q1 & Q3:How do you monitor and maintain it? *7*

Q4:Running at the Z? *7*

C. Calibration of the Energy Response of the HADCAL *8*

Q1: Give an outline of the plan for calibrating the energy response of your calorimeter, both from test beams or monitoring signals and in situ running. *8*

Q2:What level of precision is required? How is it obtained? *9*

Q3:Monitoring of the calibration *9*

Q4:Operation at the Z pole *9*

References *10*

III. Answers to Questions about Tracking **11**

A. Questions Re Tracker Alignment 11

Q1: What is your plan for aligning your tracking systems? *11*

Q2: What is the precision required? *17*

Q3: Are there special operations needed for alignment after push-pull prior to data taking, and what time is required? *18*

Q4: How many degrees of freedom need to be considered after a move? *18*

Q5: How do the alignment needs affect the design of your detector? *19*

Q6: Is any real-time monitoring of the tracker alignment envisioned (e.g., related to power pulsing and long term stability)? *20*

B. Questions and Answers Re Tracking Robustness 22

Q1: Elaborate on the robustness and redundancy of the tracking performance. In particular, how would it deteriorate with a missing layer? *22*

Q2: Give the efficiency and the fake track fraction in a jet environment with full background simulation. *31*

C. References 32

IV. Answers to Questions about Benchmarking 33

A. IDAG Questions about Benchmarking 33
B. Generation and Processing of Data to Answer Benchmarking Question 33
C. (Q1)Re-analysis of Higgs Recoil Mass and Cross Section with Corrected ISR Spectrum and Simulation of Beam Background Hits 37

1. Re-analysis of $e^+e^- \rightarrow ZH \rightarrow l^+l^-H$ with Corrected ISR Spectrum 37
2. Analysis of $e^+e^- \rightarrow ZH \rightarrow l^+l^-H$ including a Simulation of Beam Background Hits 41

D. *(Q2)* Higgs Recoil Mass and Cross Section Analysis in the eeH Channel with and without Calorimeter Recovery of Bremsstrahlung Photons 41
E. *(Q3)* Calibration of the template analysis for mass resolution in t-tbar and neutralino/chargino channels 43

V. Answers to Questions about MDI 50

A. Questions & Answers 50

Q1 - Numerics: Please, check the summary table (MDIsummary.xls) and correct any factual errors, or provide the missing numbers, in particular, for the items that follow – *50*

Q2 - Footprint: Please, indicate the envelope (or footprint) that the detector has to occupy during the maintenance period in the offline position. *50*

Q3 - Shield blocks: Please, provide the rough size of additional shield blocks to use and their schematics (if they exist), when the detector is in the online position. The objects to consider include: pacmen, shield walls, others. *50*

Q4 - Platform and height: Please, indicate the assumed height of the platform beneath the detector, its size, its weight, and the assumed beamline height relative to the detector hall floor. *50*

Q5 - Gross weight: Please, indicate the gross total sum of the weight of your detector system, including the barrel, endcaps, platforms (if any), and shield blocks. *50*

Q6 - QD0: Please, indicate the Z locations of your QD0 (Zmin and Zmax) and their radius R to occupy. *50*

Q7- Cryogenics: Please, indicate if your QD0 and the solenoids are to operate at 2K or 4K. *50*

Q8 - Push-pull motion: *51*

MDI figures: *53*

List of Figures

Figure 1. 1 6
Figure 3. 1 14
Figure 3. 2 15
Figure 3. 3 16
Figure 3. 4 24
Figure 3. 5 25
Figure 3. 6 26
Figure 3. 7 28
Figure 3. 8 29
Figure 3. 9 29
Figure 4. 1 38
Figure 4. 2 39
Figure 4. 3 41
Figure 4. 4 42
Figure 4. 5 44
Figure 4. 6 45
Figure 4. 7 47
Figure 4. 8 48
Figure 5. 1 53
Figure 5. 2 54
Figure 5. 3 55

List of Tables

Table 3. 1 30
Table 3. 2 31
Table 4. 1 40
Table 4. 2 40
Table 4. 3 43

I. Introduction

A. What this document is

Following the submission of the Silicon Detector (SiD) Letter of Intent and its initial review by the International Detector Advisory Group (IDAG) at the TILC09 meeting in Tsukuba, Japan in mid-April, 2009, a series of questions were forwarded from the IDAG to SiD, in the expectation that answers would be provided in advance of the IDAG's planned meeting in Orsay on June 19-21, 2009. This document is a compilation of those answers.

B. The IDAG questions

For all three concept groups:

1. Give an outline of the plan for calibrating the energy response of your calorimeter, both from test beams or monitoring signals and *in situ* running. What level of precision is required? How is it obtained? How do you monitor and maintain it? If operation at the Z pole is part of your strategy, how much data is required?

2. What is your plan for aligning your tracking systems? What is the precision required?

3. Are there special operations needed for alignment after push-pull prior to data taking, and what time is required? How many degrees of freedom need to be considered after a move? How do the alignment needs affect the design of your detector? Is any real-time monitoring of the tracker alignment envisioned (e.g., related to power pulsing and long term stability)?

4. Repeat the recoil analysis with Z -> μ+μ-, e+e-, including the corrected ISR spectrum, and simulation of beam-background hits.

For the SiD concept:

5. Elaborate on the robustness and redundancy of the tracking performance. In particular, how would it deteriorate with a missing layer? Give the efficiency and the fake track fraction in a jet environment with full background simulation.

6. Calibrate the template analysis for mass resolution in t-tbar and neutralino/chargino channels: study the robustness of the method by adding more comparison tables.

7. Z(e+e-)H inclusive: show the result of the analysis with and without the calorimeter

In addition to these questions from the IDAG proper, the IDAG members concerned with MDI issues forwarded additional questions as follows:

Questions for LoI Groups on MDI-related Issues from IDAG

1. Numerics: Please, check the summary table (MDIsummary.xls) and correct any factual errors, or provide the missing numbers, in particular, for the items that follow –

2. Footprint: Please, indicate the envelope (or footprint) that the detector has to occupy during the maintenance period in the offline position.

3. Shield blocks: Please, provide the rough size of additional shield blocks to use and their schematics (if they exist), when the detector is in the online position. The objects to consider include: pacmen, shield walls, others.

4. Platform and height**:** Please, indicate the assumed height of the platform beneath the detector, its size, its weight, and the assumed beamline height relative to the detector hall floor.

5. Gross weight: Please, indicate the gross total sum of the weight of your detector system, including the barrel, endcaps, platforms (if any), and shield blocks.

6. QD0: Please, indicate the Z locations of your QD0 (Zmin and Zmax) and their radius R to occupy.

7. Cryogenics: Please, indicate if your QD0 and the solenoids are to operate at 2K or 4K.

8. Push-pull motion:

   a) Please, indicate the preferred method of push-pull motion mechanics that is currently under consideration.

   b) Please, identify the hardware components (beamline elements, shield blocks, and utilities) that need to be disconnected/disassembled and reconnected/reassembled during your detector push/pull. Please, estimate how long this relocation / reassembly work will take.

   c) Assuming that the accelerator (including QF1) is in a good alignment condition, how long would it take to complete your detector "push", and complete the alignment of the detector components. Explain how you will do this realignment; i.e. what kind of measurement and mover systems.

   d) How long would it take to complete your detector "pull" and to make the interaction region and the BDS ready for the other detector?

   e) During the upcoming Technical Design Phase, what type of resources do you plan to allocate for the conceptual and engineering work on MDI-related issues, and how you intend to operate them? Also, do you have any requests for assistance to the RD management or to the MDI group, in terms of resource sharing or in terms of interactions on technical matters?

C. Organization of this document

All these questions are dealt with in the following sections of this document, as follows: In Section II, the answer to the first question about calorimeter calibration is given. In Section III, the answers to questions about tracking, both alignment and robustness and tracking performance, are given. Section IV discusses the benchmarking issues, including a repeat of the recoil Higgs analysis, the utility of the calorimeter in the recoil analysis in the case of Z decay to ee, and the calibration of the template analysis techniques which was used in the SiD LoI. A discussion of the Monte Carlo data generated for answering these issues is included as well. Section V is devoted to the MDI questions. Some conclusions are presented in Section VI.

II. Answers to Questions about Calorimeter Calibration

A. The questions from IDAG

1. Give an outline of the plan for calibrating the energy response of your calorimeter, both from test beams or monitoring signals and *in situ* running.
2. What level of precision is required? How is it obtained?
3. How do you monitor and maintain it?
4. If operation at the Z pole is part of your strategy, how much data is required?

This section consists of two sections, outlining the calibration for the electromagnetic (emcal) and the hadronic (hadcal) calorimeter. Each of the questions raised is addressed below.

B. EMCal Response

Q2:What level of precision is required?

The most demanding conceivable requirement is given by the stochastic term for an e^+e^- or $\gamma\gamma$ final state at a 1 TeV collider: $\frac{17\%}{\sqrt{500}} = 0.8\%$

There is no known physics case for the above. Such simple final states are easily identified and the energies are known by the beam energy (or by the beam energy combined with the position measurements in the case of a radiative event). In fact, the resolution for such a high energy shower would require a significant longitudinal leakage correction, which is certainly tractable given the certainty for modeling of electromagnetic shower shapes, but again, is not required by the physics.

We certainly do not want the EM energy resolution to contribute non-negligibly to the jet energy resolution. So given typical photon energies in jets of $\sim$10 GeV, one can assign conservatively a required resolution of $\frac{17\%}{\sqrt{50}} = 2.4\%$. However, we can take the extreme case above as a goal.

So we take 2% as a requirement, but choose $< 1\%$ as a goal.

Q2:How is it obtained?

We have used both EGS4 and Geant4 to model the EMCal and obtain the response and stochastic resolution term. The systematic term is limited fundamentally by the choice of silicon as the sensing elements. The KPiX readout electronics is calibrated pixel-to-pixel by an accurate built-in system. The absolute calibration and the sensor-to-sensor variation is determined initially using radioactive sources and IR laser, and is checked using a test beam. The tungsten thickness is controlled to 0.5%.

The response of a silicon detector is very stable and is quite insensitive to all parameters which control its operation. Sensor-to-sensor response variations are controllable in production and should be quite small, but nevertheless can be measured by straightforward techniques. Silicon-tungsten systematics have been shown to be well controlled (~ 0.1% systematic error) in the luminosity calorimeters of several experiments at LEP/SLC. The response of a calorimeter layer depends on the thickness of the tungsten plates, the thickness of the active area in silicon detectors (depletion depth), and the electronics calibration. Determining the pixel-to-pixel and sensor-to-sensor variations in the electronic response is expected to be the greatest challenge, but seems to be tractable. These issues are addressed below:

- *silicon sensor depletion depth*

  We expect to supply bias voltage to the silicon well in excess of that needed to fully deplete them. As a result the active thickness of the silicon will be extremely stable. The thickness of the detectors can easily be measured and is controlled to a few micron in production. For 0.5% precision we would need to measure the thickness of the sensors with a precision of 1.5 microns.

- *tungsten plates thickness*

  We expect to use the rolling process. The average thickness of the plates can be controlled to better than 0.5% by weighing them. The dimensions can be monitored. The fabrication should be able to maintain this same dimensional accuracy.

- *electronics calibration - absolute*

  The sensor plus KPiX response will be measured using both radioactive sources and IR laser. We anticipate taking data with a radioactive source for a select number of pixels for all sensors. A candidate source is the 60 KeV gammas from ^{241}Am, for which a spectrum taken with our sensors is shown in Figure 1.1. Other sources with higher energies might also be useful. But this has yet to be determined in the lab.

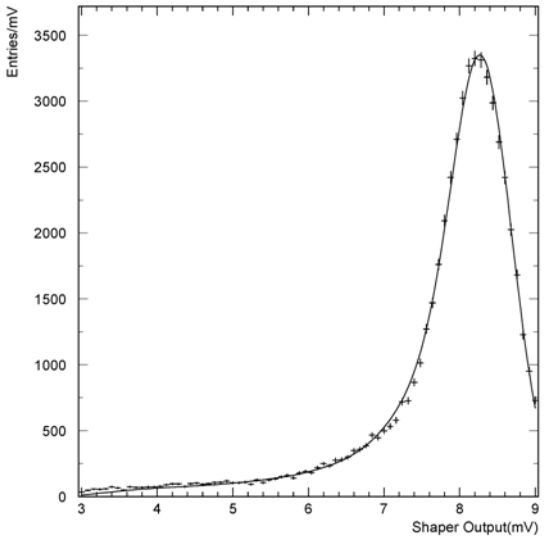

Figure 1.1 Spectrum of ^{241}Am source taken with our sensors.

We also will measure the response of a limited number of pixels per sensor with an IR laser. This has the property of leaving an ionization trail which penetrates the full sensor, as for a MIP. Hence we can cross-check the source measurements and provide an absolute calibration of depletion depth. We have demonstrated the usefulness of the IR laser in the lab up to an equivalent of 40 MIPs, thus probing both the high- and low-gain ranges of the KPiX.

All of the above must be carried out before assembly of calorimeter modules. However, in the case of modules for beam tests, one imagines that the modules can be disassembled for follow-up source measurements. We have checked in simulation that the resolution is insensitive to the value of the electronics threshold, as long as it is uniformly applied. We plan to check this in a beam test. Response linearity is expected to be excellent for the sensors. The KPiX response linearity is probed using the built-in calibration. This will ultimately be checked in the beam test.

- *electronics calibration – variations*

  The pixel-to-pixel calibration of KPiX depends on the combination of calibration and signal-hold capacitors. These are laser trimmed. Recent measurements with KPiX-7 indicate that the capacitance values are uniform to ~0.1%. This needs to be confirmed by making source measurements for all pixels of a limited number of sensors. Random variations at this level will have a negligible contribution on performance.

  Sensor-to-sensor calibration will again be determined initially with a radioactive source and the IR laser.

- *test beam*

  The procedure above will be used to construct and calibrate a test beam module. The beam test will provide a system test. We do not expect to require carrying any specific calibration results from the beam test to the final calorimeter. Indeed, if the test beam results confirm expectations, then we would repeat the above procedures for the SiD EMCal. If they do not, then we will investigate and identify the error(s) in the procedure before advancing to the SiD EMCAL. In reality, this opportunity will likely be afforded by an intermediate step in which a full mechanical module is fabricated and tested in a beam.

Q1 & Q3:How do you monitor and maintain it?

The Bhabha scattering process provides a nearly ideal in-situ calibration source. Even at $\theta = 90^o$ we will have more than 1 Bhabha electron per sensor per fb^{-1}. The rate is larger at smaller angles. The typical Bhabha electron has known energy and back-to-back topology. Even the radiative Bhabhas are typically constrained kinematically and can be used to check the linearity of the response. The Bhabhas will provide the absolute calibration and its variation over distance scales greater than about 20 cm. It will probe all calibration effects.

Perhaps the main drawback to Bhabhas is that, because of their high energy, there will be significant longitudinal leakage of Bhabha showers. However, the variation in this leakage through the calorimeter is small and can be readily modeled since electromagnetic shower shapes are well understood. In addition, the full dynamic range of all layers will not be probed equally with this method. However, since the main resolution issue is for EM showers, this calibration is well matched. But it may be useful to also use charged pions before showering (MIPs) as an additional calibration source.

Q4:Running at the Z?

We would not require running at the Z, but we would certainly make good use of it if it were available.

C. Calibration of the Energy Response of the HADCAL

Q1: Give an outline of the plan for calibrating the energy response of your calorimeter, both from test beams or monitoring signals and in situ *running.*

This note addresses the calibration procedures for a Digital Hadron Calorimeter (DHCAL) with Resistive Plate Chambers (RPCs) as active media. The readout of the RPCs is assumed to be segmented into 1 x 1 cm^2 pads, which are read out individually with a resolution of 1-bit (digital readout). With this fine granularity of the readout, the entire DHCAL will count approximately $5 \cdot 10^7$ readout channels.
Additional details concerning the calibration procedures can be found in ref. [1].

The event record for the DHCAL contains a list of hits and their location. It is assumed that an algorithm, e.g. a PFA, assigns subsets of these hits $\sum H_i$ to individual hadronic showers. The energy E_h of such a shower will be reconstructed as

$$E_h = \alpha^h_{sampl} \times \sum_i \left[\left(H_i - B_i\right) \times \frac{\varepsilon_0}{\varepsilon_i} \times \frac{\mu_0}{\mu_i} \right]$$

$$= \alpha^h_{sampl} \cdot \varepsilon_0 \mu_0 \times \sum_i \frac{H_i - B_i}{\varepsilon_i \mu_i}, \qquad (Eq.1)$$

where

H_i … are the hits in layer i assigned to a given shower, where i runs over all layers of all modules of the DHCAL,
α^h_{sampl} … is the sampling term, which may depend on ΣH_i,
B_i ... is the average contribution from noise in layer i of the geometrical area of the shower,
ε_0 … is the average MIP detection efficiency of all RPCs in the calorimeter,
ε_i … is the actual MIP detection efficiency of layer i,
μ_0 … is the average pad multiplicity for a MIP of all RPCs in the calorimeter, and
μ_i … is the actual pad multiplicity for a MIP in layer i.

Equation 1 contains six calibration constants/variables. Of these, three constants (α^h_{sampl}, ε_0, μ_0) are time-independent and three variables (B_i, ε_i, μ_i) may vary with time. Whereas the time-independent constants need to be determined only once as part of the calorimeter's calibration procedure, the time-dependent variables need to be monitored during the entire data taking period.

The default MIP detection efficiency ε_0 and pad multiplicity μ_0 will be chosen such as to correspond to reasonable operating conditions, i.e. high voltage and readout threshold setting, for the chambers. Ideally, their values will remain constant for the life of the experiment.

The sampling term α^{h}_{sampl} will be determined from test beam data (for charged pions) and from a validated Monte Carlo simulation of hadronic showers (for neutral hadrons).

Cross-checks of the calibration of the DHCAL will be obtained with measurements of back-to-back jets and reconstructed W-boson masses. Additional cross-checks will be provided by comparison with the momentum measurement of isolated charged hadrons.

Q2:What level of precision is required? How is it obtained?

Based on detailed simulations of the response of RPCs, the effect of uncertainties in the calibration on the measurement of single particle energies was estimated. The studies showed that, for instance, for 10 GeV π^{+} the energy resolution degrades by approximately by 1%, if the entire module's response is smeared by a Gaussian distribution with a sigma of 3%. This is the worst case scenario, where the responses of all layers in a given module are 100% correlated. If, on the other hand, all individual layers in a module fluctuate independently say by a Gaussian distribution with a sigma of 3%, the effect on the energy resolution is negligible.

From these studies we conclude that a calibration of the DHCAL with a precision at the 3% level is more than sufficient.

Q3:Monitoring of the calibration

The time-dependent variables will be monitored during the entire data taking period. Based on our experience with a small size prototype calorimeter, we assume that the variations in response are uniform over an entire chamber. The average contribution from non-beam related background hits will be measured with self-triggered data. The beam-related background contributions (e.g. from neutrons) will be estimated using bunch-crossing events and algorithms for separating the energy deposits from e+e- collisions and from beam backgrounds. The MIP detection efficiency ε_i and pad multiplicity μ_i will be determined with cosmic rays and track segments in hadronic showers. Each method is expected to provide the requested 3% precision within one week. In addition, corrections for changes due to changes in environmental conditions will be applied to interpolate between measurements of ε_i and μ_i.

Q4:Operation at the Z pole

Operation at the Z-pole is not required, but will certainly be used if it is available.

References

[1] “Calibration of a Digital Hadron Calorimeter with Resistive Plate Chambers as Active Media”, J. Repond and L.Xia

III. Answers to Questions about Tracking

A. Questions Re Tracker Alignment

1. What is your plan for aligning your tracking systems?
2. What is the precision required?
3. Are there special operations needed for alignment after push-pull prior to data taking, and what time is required?
4. How many degrees of freedom need to be considered after a move?
5. How do the alignment needs affect the design of your detector?
6. Is any real-time monitoring of the tracker alignment envisioned (e.g., related to power pulsing and long term stability?

Q1: What is your plan for aligning your tracking systems?

Overall strategy:

The alignment strategy for the SiD outer tracker, vertex detector, and beam-pipe assemblies is based on 1) a small number of robust, rigid elements; 2) precise positioning of smaller components during fabrication and assembly; 3) real-time monitoring of alignment changes, including during push-pull moves; and 4) track-based alignment for final precision. Because alignment at the level of O (few μm) is important to exploit the intrinsic resolution of the SiD tracking system, determining alignment from several methods with different systematic errors is a prudent strategy. Below we describe the several planned methods that should give us confidence that we understand the detector's alignment to the required precision. But in brief, we expect to achieve ~20 μm relative precision among outer tracker sensor modules in different layers after fabrication and assembly in the full detector. The final precision of a few μm is attained for individual sensor modules from track-based alignment, with real-time FSI and laser-track monitoring providing both a hierarchical bridge from the coarse to the fine alignment and a set of global corrections for time dependent structure motion and deformation.

The first time this full alignment is attempted, we will likely need several weeks of collider data taken with at least modest luminosities to achieve good alignment precision, but subsequent re-alignments following push-pull operations should proceed rapidly, using the FSI and laser-track systems, since the stability of the relative sensor positions is expected to be better than the measurement precision of these alignment systems. In other words, a large number of detected tracks will be essential for initial tracker alignment, but for subsequent alignments, detected tracks will be used to provide a cross-check. Design luminosity at a center-of-mass energy of 500 Gev (or even two orders of magnitude lower luminosity) should nonetheless be adequate for determining alignment. Dedicated running on the Z pole could be useful, but is not thought to be necessary for successful tracker alignment.

Fabrication and assembly

Tracker alignment begins during tracker fabrication and assembly. Sensor alignment within each outer tracker module will be measured with respect to fiducials and mounting features of the module. Modules will be solidly anchored with stable relative position to stiff support cylinders and support disks, which are based upon carbon fiber laminate material. That material provides good thermal stability and should give a rigidity for the SiD tracker that is ~50 times higher than that of the CMS tracker. Predicted deflections of the support structures under gravity are small: < 10 μm. Modules will be installed in groups with internal alignment of a group controlled to ~ 10 μm. Reference features on each barrel and disk will allow the positions of each group of modules to be known with respect to the reference features to ~ 10 μm. Hence position and orientation of a given sensor should be known to approximately (10 μm) * $3^{0.5}$ = 17 μm. A large coordinate measuring machine or equivalent laser-based equipment will be needed to achieve this accuracy. Frequency scanned laser interferometry during assembly offers the potential for still better knowledge of alignment than the values above. In the end, knowledge of alignment is more important than precision positioning.

We plan to use ball and cone mounts to mate barrels and disks with one another. That type of mount provides a reproducibility of ~ 3 μm. Again, a large CMM or laser-based equipment will be used to measure reference features on each object. Precision should be ~ 10 μm, which implies the precision to which individual sensors are known to ~ 20 μm, although individual groups of sensors will be known relative to one another with slightly better precision.

Within the Silicon Detector, kinematic mounts will be used to support the outermost tracker barrel from the interior of EMCAL. Support via kinematic mounts from some other portion of the detector has also been considered. All other outer tracker elements are supported either directly or indirectly from the outermost barrel. If the kinematic mounts are done correctly, push-pull operations may affect absolute position of the tracker, but should not affect tracker internal alignment.

The vertex detector is supported independently of the outer tracker. Outer support half-cylinders locate all vertex detector elements relative to one another. Relative alignment of elements within either top or bottom support cylinder is likely to be better than half-cylinder to half-cylinder alignment. That suggests the two half-cylinders and detector elements they support may need to be treated as independent objects.

Then the tracker would be treated as three pieces: the outer tracker (including all barrel layers and disks), the upper half of the vertex detector, and the lower half of the vertex detector. Within each of these we would hope to provide support which ensures good internal alignment. Alignment of the three pieces relative to one another will be monitored via frequency scanned interferometry (FSI). A combination of frequency scanned interferometry and "laser-track" monitoring of relative sensor positions will monitor internal alignment of the outer tracker. That type of monitoring may not be

feasible for internal alignment of the two vertex detector halves due to constraints on the material budget.

After assembly, during data taking, and during push-pull operations, the FSI system will be run nearly continuously, providing ``real time'' measurement of global tracker distortions and of vibration amplitudes and frequencies (up to the Nyquist frequency – O (kHz) of the FSI DAQ sampling).

A deformation monitoring system based on optical fiber sensing techniques is also under consideration. Strain Optical Fiber Sensors (OFS) would be embedded in the carbon fiber supporting structures or/and sensor modules. The OFS would provide real-time strain information during the production, assembly, operation and push-pull operation of the instrumented tracker structures. From a detector integration point of view, using this kind of distributed monitoring requires only the embedding of 120-um diameter optical fibers in the carbon fiber composite; this means that it can be also considered as a suitable technology for the vertex detector.

Frequency scanned interferometry

The FSI system incorporates multiple interferometers fed by optical fibers from the same laser sources, where the laser frequency is scanned and fringes counted, to obtain a set of absolute lengths [1,2]. This alignment method was pioneered by the Oxford group on the ATLAS Experiment. By defining O(100's) "lines of sight" in the tracker system for absolute distance measurements, we will overconstrain the locations of fiducial points in space, allowing global distortions of the carbon-fiber support structure layers (translation, rotation, twist, bending, stretching, etc.) to be determined to the required precision. Figure 3.1 shows an extreme example with many lines of sight for one barrel layer from a study done some years ago on a SiD precursor design. The real-time FSI measurements should allow for relevant time-dependent corrections to be applied when carrying out the final step of track-based alignment of individual silicon modules.

With a test apparatus, the state of the art in precision DC distance measurements over distance scales of a meter under laboratory-controlled conditions has been reached and extended. Precisions better than 100 nm have been attained using a single tunable laser when environmental conditions are carefully controlled. Precisions under uncontrolled conditions (e.g., air currents, temperature fluctuations) were, however, an order of magnitude worse with the single laser measurements.

Hence a dual-laser FSI system is foreseen for the tracker, one that employs optical choppers to alternate the beams introduced to the interferometer by the optical fibers. By using lasers that scan over the same wavelength range but in opposite directions during the same short time interval, major systematic uncertainties can be eliminated. Bench tests have achieved a precision of 200 nm under highly unfavorable conditions using the dual-laser scanning technique. Figure 3.2 shows an example of dual-laser fringes measured on a bench-top single-channel prototype system.

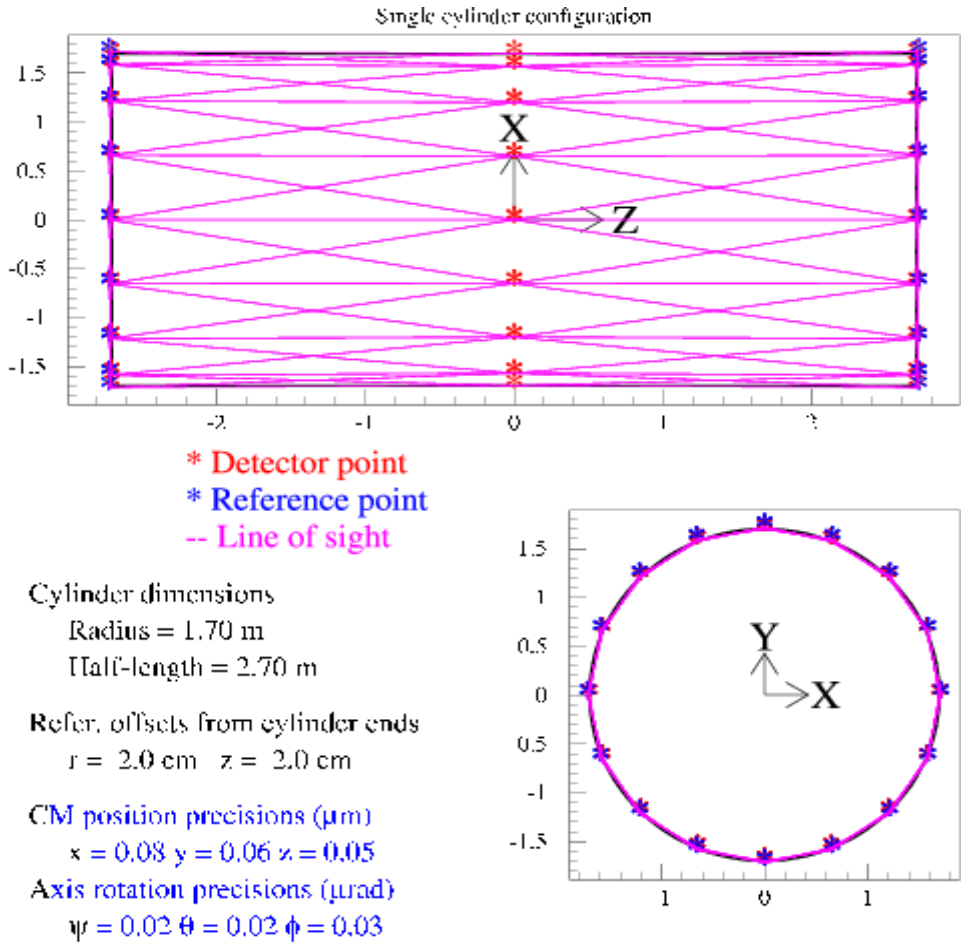

Figure 3.1 Example of lines of sight for one barrel layer, taken from a study of an SiD precursor design, along with achievable fitted precisions on center-of-mass offsets (μm) and pitch/yaw/roll rotations (μrad). This example is somewhat extreme (~100 lines of sight for a single layer) and permits greater positional and pointing precision than is needed.

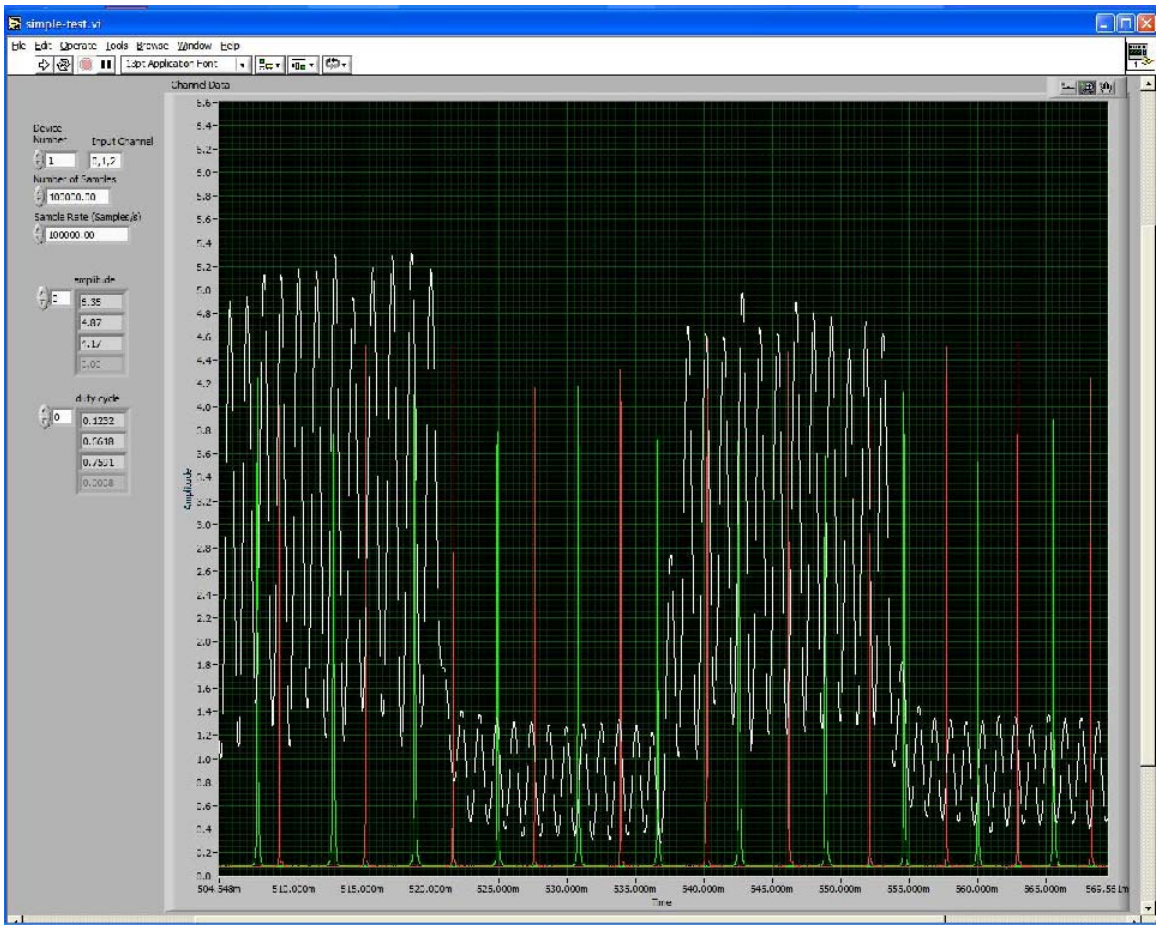

Figure 3.2 Example of FSI fringe display for a single-channel dual-laser FSI system. White peaks indicate interference fringes, while red and green peaks are Fabry-Perot transmission maxima from a chopped, dual-laser system.

It should be noted that the FSI data can be analyzed in complementary ways, either to minimize sensitivity to vibrations, in order to determine accurate mean shape distortions, or to maximize sensitivity to vibrations below the Nyquist frequency O(kHz) of the data sampling, in order to study transient effects. In particular, vibrations due to pulsed power operation can be investigated, as discussed below in the response to question 6.

Laser-track method

A separate real-time alignment method with different systematic uncertainties will be provided by a "laser-track" system in which selected sensor modules are penetrated by laser beams to mimic infinite-momentum tracks. This method exploits the fact that silicon sensors have a weak absorption of infrared (IR) light. Consecutive layers of silicon sensors are traversed by submillimeter IR laser beams, as indicated in Figure 3.3, which can be located with few micron precision. Then the same sophisticated alignment algorithms as employed for track alignment with real particles can be applied with arbitrarily high statistics to achieve relative alignment between modules to better than a

few microns. This method employs the tracking sensors themselves, with only a minor modification to make them highly transparent to infrared light. Only the aluminum metalization on the back of the sensor needs to be swept away in a circular window with a diameter of few millimeters to allow the IR beam to pass through. Since IR light produces a measurable signal in the silicon bulk, there is no need for any extra readout electronics. This alignment method has been implemented by both the AMS and CMS Experiments.

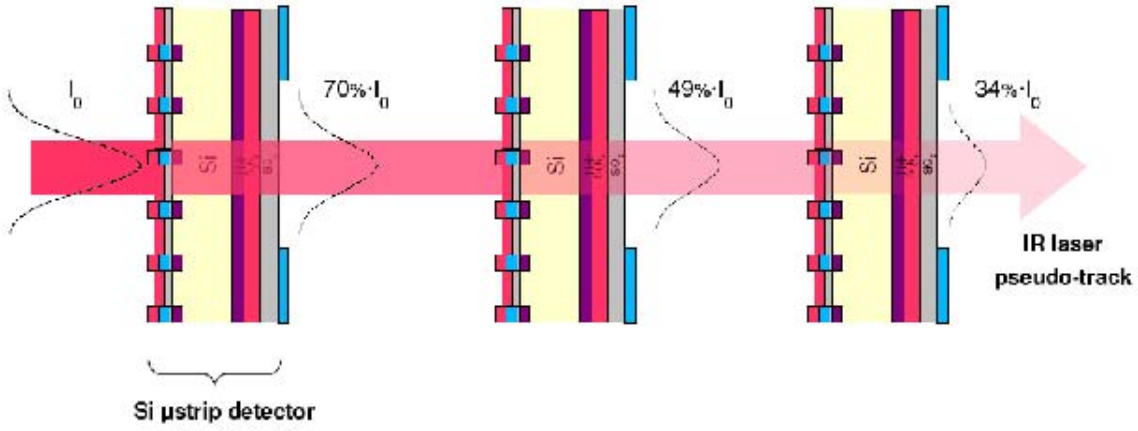

Figure 3.3 Sketch of the IR alignment method

A key parameter to understand the ultimate resolution of this method is the transmittance of a silicon sensor and the diffraction of the light. As a first approximation a silicon sensor is viewed as a stack of perfectly homogeneous plano-parallel layers, each characterized by its index of refraction and thickness. The layers are, however, not continuous, but present local features, so that diffraction phenomena will appear if the size of the obstacle is comparable to the wavelength used. For instance, the strips of the detector, pitched every 10 to 50 μm are good examples of an optical diffraction grating for an incoming beam in the IR. It has been determined that a key parameter determining the overall transmittance of a microstrip detector is the pitch to strip ratio, that is, the fraction of the strip covered by aluminum. The smaller the strip width, the more light is transmitted. It was determined that good transmittance was achieved when the strip width was set to 10% of the pitch. Tuning of sensor thickness was found to contribute up to 5% over the layout optimized value. In bench tests, based on CMS strip detectors, a relative alignment of a few microns has been achieved.

Optical Fiber Sensor deformation monitor

The sensing element of the OFS monitor is a Fiber Bragg Grating (FBG) sensor operated as an optical strain gauge. FBG sensors have many enhanced features with respect to traditional electrical strain gauges: no need for power or readout cabling, long term stability, immunity to electromagnetic fields, high voltage, extreme temperature and radiation resistant. Concerning its application in tracker systems, one of the most important properties is its light weight since the actual FBG is “written” in a few

millimeters section of an optical fiber with a 125 μm diameter. Multiplexing capabilities having many distributed FBG sensors on the same optical fiber are available; this technology also allows for long-range sensing, placing the read-out unit well outside of the detector.

The FBG sensor would be embedded in the carbon fiber structures supporting the modules and the module mechanics itself. The system is expected to reach local deformation sensitivities better than 1 μstrain. The OFS monitor will provide a very fast feedback on full structure deformations during the push-pull operations.

Track-based alignment

The final alignment of individual sensor modules will be track-based, using accumulated statistics from many detected tracks and constrained fitting to determine local position and orientation corrections for that module. (The time to accumulate sufficient statistics for alignment of each individual module is expected, however, to be long enough to require continuous monitoring of global structure motions and deformations via the FSI and laser-track systems and to warrant robust, stable mechanical structures, as discussed above.) Although six parameters are needed, in principle, to describe a rigid module's position and orientation, the most critical parameter by far for microstrip planes is the offset of the module from nominal along the direction normal to the microstrips and in the module plane, since this is the coordinate measured most precisely by the strips. Expected translations in the orthogonal directions should have a negligible effect on track. Rotations of module planes about their normals and about an axis parallel to the strips can lead to small biases in coordinate reconstruction, while rotation about an axis in the module plane and perpendicular to the strips should have negligible effects.

Determining these translations and rotations from minimizing residuals in fitted tracks requires adequate statistics for each module. To determine systematic offsets in the measured coordinate to a precision that is an order of magnitude smaller than the hit resolution requires O(100) tracks per module (assuming systematic variations in hit reconstruction for different strips in the same module are negligible). A study presented at the LCWS2006 [3] suggests that at ILC design luminosity, the sensor modules receiving the least number of tracks [$\cos(\theta) = 0$, outer barrel layer] will be penetrated by $O(10^4)$ tracks per month, making track-based alignment feasible for each separate data-taking epoch between push-pull moves, even well below design luminosity. The fact that a large number of tracks produced will be back-to-back in the x-y plane with approximately equal p_t values should enable more powerful constrained-fit determination of module offsets.

Q2: What is the precision required?

Benchmarking studies, which have been given high priority, have typically assumed perfect detector alignment. Simulation studies to answer this question thoroughly remain to be completed, but studies to date indicate we should aim for 3 μm or better on outer tracker transverse coordinate offsets (barrels and disks) for an assumed hit precision of 7 μm. We believe attaining this alignment precision would result in negligible decreases in

the extremely good resolution silicon can provide. We expect actual requirements based upon simulation results to be looser.

Vertex detector alignment is even more demanding, given that the expected single hit resolutions for both coordinates is ~3 μm. A coordinate measuring machine can provide a discrete precision per coordinate of ±2 μm, which corresponds to a sigma of 1.15 μm, but monitoring stability of alignment will be critical, both internally via tracks and with respect to the outer tracker via the FSI system. We will aim for 1 μm relative alignment precision for coordinates transverse to tracks.

Q3: Are there special operations needed for alignment after push-pull prior to data taking, and what time is required?

During detector moves, alignment of the beam pipe, the ends of the outer tracker, and the positions of the lumical and beamcal will be monitored nearly continuously relative to the central calorimeter via frequency scanned interferometry. At the end of the move, alignment of the beam pipe, the lumical and beamcal, and the final quads will be adjusted and determined relative to the outer tracker and central calorimeter. The vertex detector is mounted from the beam pipe and follows its motion. This process should take less than two hours. No adjustments to the position of the outer tracker are anticipated. Tune-up of beam position will be performed at low intensity while monitoring vertex detector and outer tracker backgrounds. The time required depends upon accelerator procedures.

During each move the FSI system will be operational and taking data continuously. Alarms will be set for any motion measured outside of what is expected. Consequently, electrical power will need to be maintained continuously for the laser system, and the optical bench will need to move with the detector. In addition, we envision embedding optical fiber sensor (OFS) in the carbon fiber support structure to measure the deformation of the structure during the move. The OFS system will allow to monitor possible fast vibrations during the push-pull procedure, thanks to its large response bandwidth. Again, alarms would be set for measured values outside the expected range.

After the push&pull move, the detector position as a whole will be determined with respect to a fixed external reference frame (like cavern walls) using survey techniques like large scale photogrametry. This is the current procedure followed by the CMS detector before and after the opening of its wheels.

Q4: How many degrees of freedom need to be considered after a move?

Precise answers to this question depend upon R&D on outer tracker, vertex detector, beam pipe, forward calorimetry, and final quad support structures. They also depend upon R&D on cabling, readout fiber optics, pulsed power, and gas cooling. Most of that R&D remains to be done. Answers which follow are best guesses based upon limited information.

Six fundamental rigid-body degrees of freedom are anticipated for outer tracker alignment after a move: two transverse positions per end, an azimuth, and a z-position. Measurement data will be collected to monitor additional degrees of freedom corresponding to shape distortions expected to be quite small (twist, bending, stretching), and to monitor long- and short-term instabilities of the rigid-body degrees of freedom.

Twelve degrees of freedom are anticipated for vertex detector alignment after a move: two transverse positions per barrel end, two transverse positions per support cylinder end, one azimuth per support cylinder end, and one z-position per support cylinder end. An additional four degrees of freedom (two transverse positions of the beam pipe near each LumiCal) will be considered in estimates of support structure distortions.

Q5: How do the alignment needs affect the design of your detector?

Support structures have been designed to minimize distortions and maintain alignment. In the outer tracker, the structure with double-walled support cylinders, concave disk support structures, and nested assembly with annular rings and kinematic mounts is intended to lead to a robust structure which can be treated as a single unit. Kinematic support from the central calorimetry is intended to minimize distortions of that structure under geometry changes of the calorimeters. R&D on prototypes remains to be done, but should allow us to verify that performance is as intended. Tracker sensor modules slightly overlap within layers (and hence are tilted), which provides valuable linking together of sensors within layers for track-based alignment.

In the vertex detector, double-walled support half cylinders are intended to preserve good internal alignment of the entire vertex detector. Since the support structures deflect under beam pipe loads, substantial R&D including measurements of prototypes will be necessary to confirm that the design works well.

Optical fibers will need to be routed carefully into the tracking region for both FSI, laser-track, and OFS systems. The FSI system will require small retroreflectors be mounted on the carbon-fiber support structure, with some retroreflectors residing in the fiducial tracking volume, including on the vertex detector support cylinder. Minimizing material burden will be important. R&D is underway to fabricate lighter retroflectors than the aluminum pellets used in the ATLAS FSI alignment system.

The laser-track method will have an almost negligible contribution to material budget. Laser fiber plus collimators will be placed outside the tracking volume. Alignment sensors for the laser-tracker will have a 1 cm diameter hole in the backside metalization but this will not affect the normal functioning of the detector. Indeed, the extension of the back-metalization does not affect the electrical behavior of the detector. On the other hand, the OFS system will not increase the material budget contribution. The optical fibers for the sensors are embedded in the carbon fiber structures. Furthermore, they will replace copper lines in the DCS system. As a byproduct, EM noise susceptibility will decrease thanks to this change.

Q6: Is any real-time monitoring of the tracker alignment envisioned (e.g., related to power pulsing and long term stability)?

Outer tracker alignment will be continuously monitored by frequency scanned interferometry, both during data taking and during push-pull moves.

At least six types of measurements are anticipated:

- Transverse and longitudinal positions of the ends of each outer tracker barrel layer at approximately eight azimuths
- Transverse positions of each barrel layer at several z-locations along the layer at approximately eight azimuths
- Overall length of each barrel layer for at least eight azimuths
- Transverse and longitudinal positions of each disk near its outer periphery for at at least eight azimuths
- Beam pipe transverse positions just inboard of each LumiCal location
- Transverse and longitudinal positions of each vertex detector support cylinder at each end (approximately four azimuths).

In addition, laser-track monitoring sensitive to movements with a time scale of seconds is planned for a subset of the sensor modules. This will allow a quick observation of relative movements between different support structures (barrel layers and disks). Its optimal layout will depend on the modularity of the support structure. An all silicon outer tracker makes integration of a laser-track system very easy. However the layout of the laser-track must try to strengthen those weak modes that affect particle track alignment. The optimal layout is under study at this moment.

The OFS deformation monitoring system can be also operated continuously. Commercial systems achieve a bandwidth higher than 1 MHz. Both the FSI and OFS systems will be valuable in monitoring possible vibrations from pulsed power operations described below.

In a 5 T solenoidal field, forces and torques acting on radial runs of power delivery cabling can be significant. Moreover, at the ILC the power is assumed to be delivered with a frequency matching the 5 Hz duty cycle of the machine. This interplay of the magnetic field with the cyclic delivery of power can result in vibrations which are transmitted from the cables into sensors and their support structures. These vibrations can be mitigated by delivering the power on flat-lines with three conductor layers. The central layer, for example, would serve to supply power and the two outer layers would serve as power returns. To avoid ground currents and ensure that supply and return currents balance within a cable, some combination of isolation of power sources and isolation of sensor grounds is needed. Then, provided the two return currents of a cable are equal, net force and torque on the cable due to interaction of currents with the magnetic field would be zero. Power/ground isolation would also eliminate issues that arise when portions of

the vertex detector are unpowered while other portions are powered. The power distribution at sensor locations should be optimized. In the barrel, radial current runs within sensors are relatively short, thereby limiting forces and torques associated with the magnetic field. In the disks, care will need to be taken to avoid supply/return current loops within sensors. In both locations, limitation of support structure material lessens the ability of those structures to resist unexpected forces and torques. It is clear that careful design and testing will be necessary to minimize the effect of potential adverse effects of the pulsed power operation on the vertex detector and outer tracker.

In any case, the effects of power pulsing on the detector alignment should be easily monitored with both the FSI and OFS systems, given their high bandwidths and precisions.

B. Questions and Answers Re Tracking Robustness

1. Elaborate on the robustness and redundancy of the tracking performance. In particular, how would it deteriorate with a missing layer?
2. Give the efficiency and the fake track fraction in a jet environment with full background simulation.

Q1: Elaborate on the robustness and redundancy of the tracking performance. In particular, how would it deteriorate with a missing layer?

Impact of a Missing Layer on Detector Resolution

We first consider the impact of a missing layer on detector resolution. We have used the Weight Matrix Fitter, which is based on the SLD track fitting algorithm, to estimate track parameter uncertainties. The covariance matrix for the track parameters is calculated by the fitter in the process of fitting tracks. This matrix does not depend on the actual hit positions, only on the amount of material along the track, the track momentum, and the spatial resolution of detector elements. Thus, we don't need a large number of tracks to get accurate calculations of the covariance matrix. For a given set of track parameters only one track needs to be propagated through the fitter to determine the covariance matrix for the fitted track parameters. We performed extensive independent studies of this algorithm to make sure that the covariance matrix gives an accurate estimate of the fitting errors. By comparing the fitted track parameters with the generated Monte Carlo track parameters, we see that the widths of residual distributions are in good agreement with the covariance matrix estimates with deviations at the few percent level.

To estimate the effect of a missing layer on tracker resolution, we have removed hits in a layer and then run the Weight Matrix Fitter to see the effect of the missing layer on track parameter resolutions. Each of the 21 layers of the tracking system – corresponding to the five vertex barrel, five tracker barrel, four vertex disk, three vertex forward disk and four forward tracker disk tracking layers – were turned off one by one. We selected 8 different polar angles for study, corresponding to cos(θ) values of 0., 0.5, 0.75, 0.8, 0.89, 0.95, 0.97, and 0.986. The results for missing any one of the 21 tracking layers on the 5 track parameters for these 8 values of polar angle as functions of track momentum in the range from 0.2 GeV/c to 1000 GeV/c can be found at http://www.slac.stanford.edu/~sinev/sid02res.html. There you will find a table with clickable links to each of the 840 variations examined. Each plot contains 2 curves, one showing the resolution with the full set of layers, and a second curve showing the resolution with the designated layer missing. In the table of links some entries are shown in blue and some in red. If the entry is red, then missing hits in that layer does not affect the resolution for that track parameter at that particular dip angle. In total, out of the 840 entries in the table, only 283 are blue indicating that missing hits in that layer could affect affect the track resolution. There is no row in the table that is completely "red", showing that each layer contributes to the tracker resolution for some region of phase space

The track parameters resolutions described above were calculated for the expected spatial resolution of the sensors. The vertex pixel sensors have a spatial resolution of 3.5 μm in both coordinates, the barrel tracker strip sensors have a spatial resolution of 7 μm in the bend coordinate, and the endcap tracker strip sensors, consisting of 2 planes of strip sensors at a 12º stereo angle, have a spatial resolution of 7 μm resolution in the bend coordinate and 35 μm resolution in the radial coordinate. It should be noted that the algorithm employed here is different from the one on which the LOI results are based. The results in the LOI (see for example Fig. 2.11) were based on a track finding algorithm without applying a subsequent track fitter. A Kalman filter had not been implemented at that point in time. The current results are based on the analytic Weight Matrix Fitter, and show a better performance of the tracking system compared to the LOI results. What is relevant for this discussion is the relative change compared to no missing layers.

As one would expect, the vertex detector layers are mostly responsible for impact parameter resolution. In the x-y plane, contrary to naive expectations, not just the first layer, but all five of the barrel layers contribute roughly equally to the impact parameter resolution at high momentum, denoted d0. This is because the "lever arm" in this case is very large due to the excellent spatial resolution in the outer tracker. For high momentum tracks, the d0 resolution is almost a factor of $\sqrt{5}$ better than the spatial resolution of a single layer. Removing any one of the vertex barrel layers leads to ~12% degradation in d0 resolution at high momentum. Things are different for low momentum particles, where the d0 resolution is dominated by multiple scattering. In that case, the first vertex layer plays the dominant role in the d0 resolution. Removing it leads to a ~50% degradation in d0 resolution, while second and subsequent layers have little effect. For the impact parameter resolution in z, denoted z0, we don't have a large effective lever arm since the barrel tracker sensors do not measure the z coordinate. Correspondingly, z0 resolution is more than a factor of two worse than d0 resolution (4 μm versus 1.8 μm at high momentum). The absence of first layer measurement degrades the z0 resolution by ~50% for all momenta. Selected impact parameter results are shown in Figure 3.4.

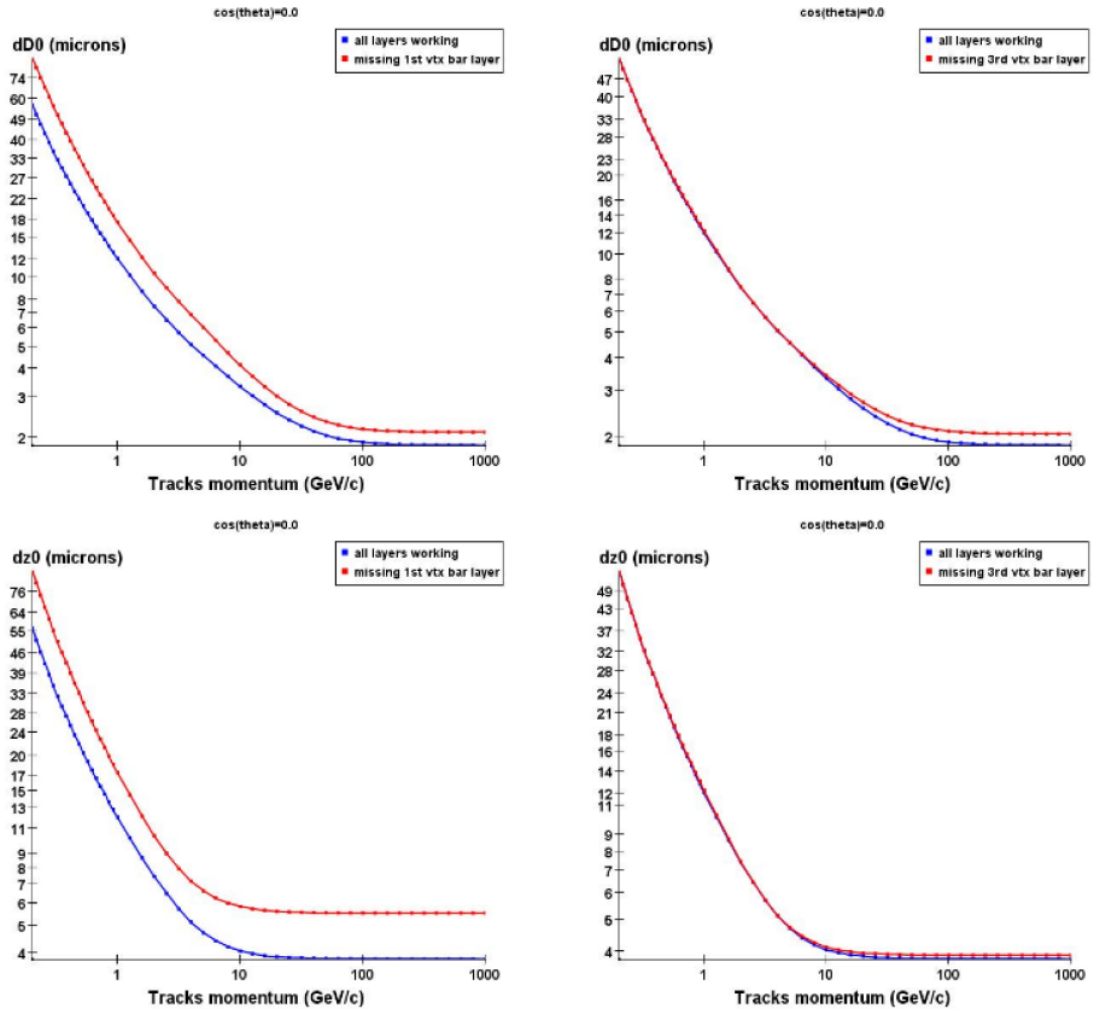

Figure 3.4 Impact parameter resolution in x-y (top) and z (bottom) for missing the first (left) and third (right) layer in the vertex detector at cos(theta)=0 (red) compared to the nominal design (blue).

The p_T resolution for the SiD tracker depends primarily on the outer tracker measurements. The vertex detector layers have little impact on the momentum resolution except for very low momentum tracks ($p_T < 0.3$ GeV/c) where the absence of the last vertex layer degrades resolution by about ~20%. Excluding hits in the first tracker barrel layer significantly degrades the resolution in the low momentum region by as much as a factor of 5. Because such tracks do not reach the next barrel tracker layer, their curvature is measured by the vertex detector alone. For $p_T > 1$ GeV/c, the most important tracker layer is the last one. Excluding hits from this layer degrades the momentum resolution by 15-20%. Selected p_T resolution results are shown in Figure 3.5.

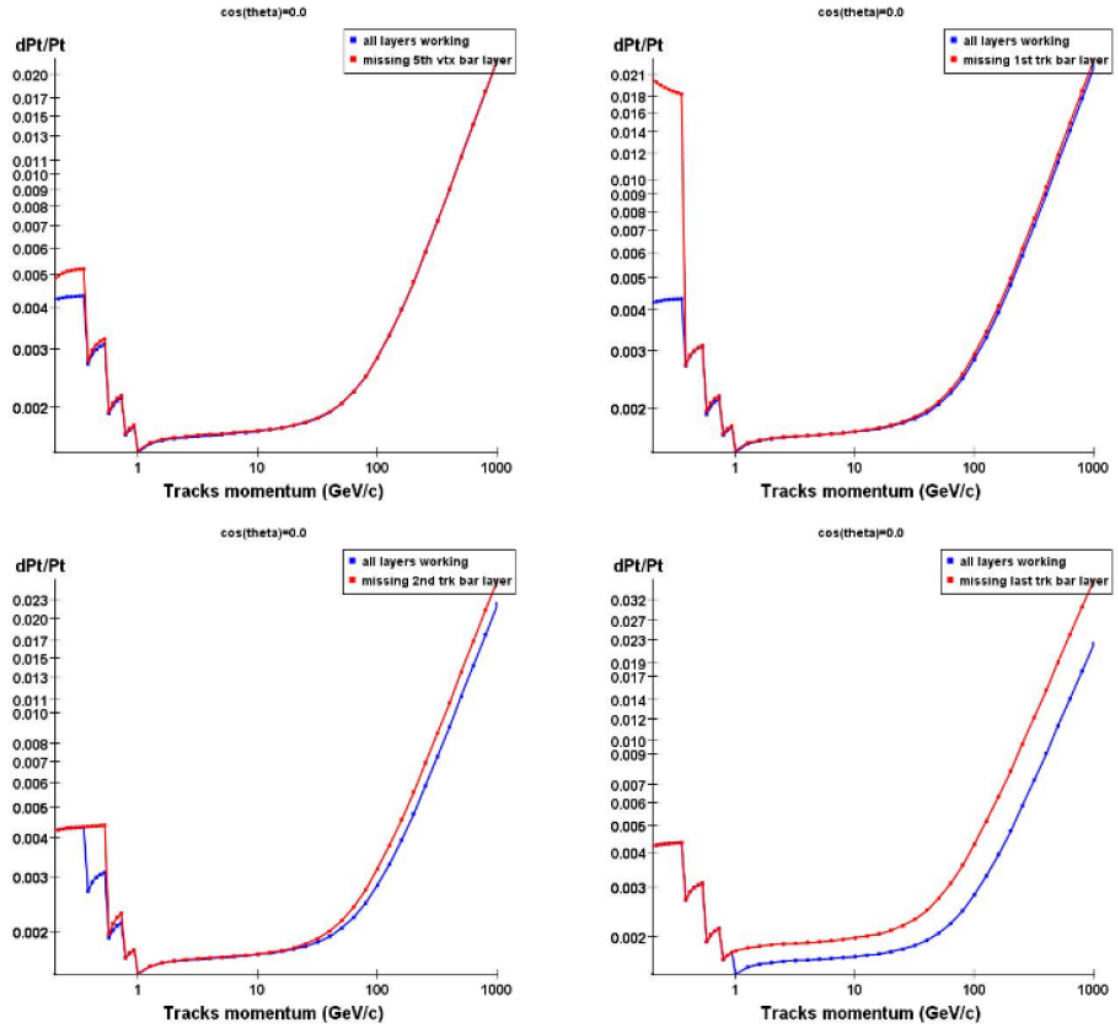

Figure 3.5 Transverse momentum resolution at cos(theta)=0 for missing the fifth vertex barrel, or first, second and last tracker barrel layer (red) compared to the nominal design (blue)

For far forward tracks ($\cos(\theta) = 0.972$), the most important layers for both impact parameter and momentum resolutions are the first vertex barrel layer and the second forward disk layer. The effect of missing these layers is shown in Figure 3.6.

In summary, the results presented above demonstrate that there is no single critical layer in SiD, the absence of which would critically impact the detector resolution. The degradation in resolution is either tolerable and limited to narrow regions of phase space (low momentum, very forward tracks) that do not significantly impact the SiD physics program. We also observe that no layer is unneeded - every layer leads to improved track resolution in some region of phase space.

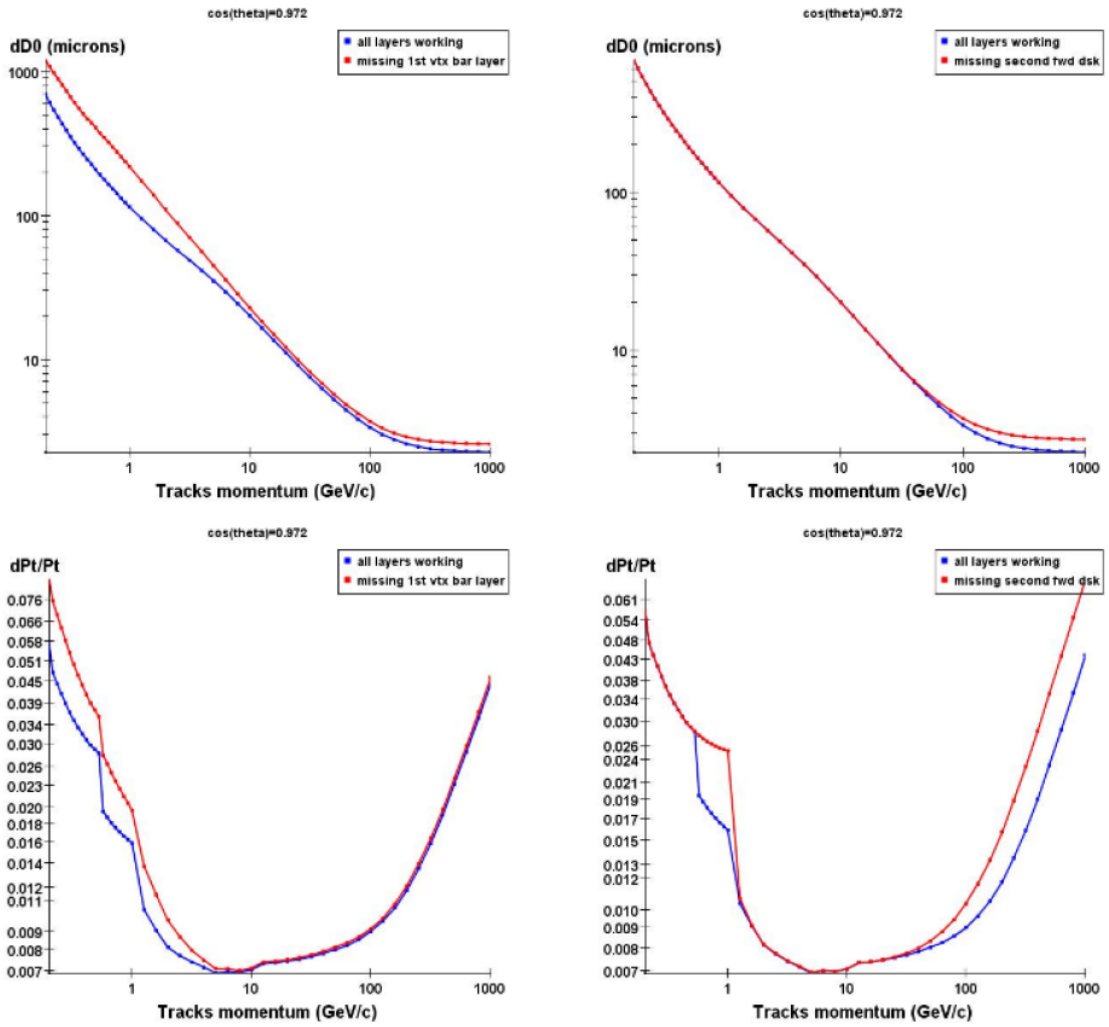

Figure 3.6 Momentum and impact parameter resolution for forward tracks with missing layers.

Impact of a Missing Layer on Track Reconstruction

We now consider the impact of a missing layer on the track finding efficiency and fake rate. We have studied 4 specific cases for a missing layer in the central (barrel) region using the baseline design with no missing layers as reference (All): missing the innermost barrel vertex detector layer (no VB0), missing the outermost barrel vertex detector layer (no VB4), missing the innermost barrel tracker layer (no TB0), and missing the outermost barrel tracker layer (no TB4). The effect of a missing layer was simulated by forcing the track finding algorithm to ignore hits on the specified layer. For each case, we generated a new set of track finding strategies using the strategy builder (see the LOI for further details on strategies and the strategy builder), using a sample of $e^+e^- \rightarrow t\bar{t}$ events at $\sqrt{s} = 500$ GeV. The tracking performance was measured using an independent sample of top pair events to avoid possible correlations between the strategy building and track reconstruction processes.

In general, we expect a missing layer to have a negligible effect on tracking performance for high- p_T tracks. Such tracks typically traverse ~10 tracking layers, while the track finding algorithms require only 6 – 7 hits. The situation for low-p_T tracks is more complex. The SiD standard tracking algorithm is not designed to follow "curlers", and will not necessarily associate hits with a track candidate after the track starts to curl back in towards the origin. Thus, low momentum tracks need to traverse the minimum number of layers (6 for a barrel only strategy, 7 for other strategies) to be reconstructed. If one of the innermost layers is missing, a substantial inefficiency arises in the current algorithm for these low-p_T tracks since the track may no longer traverse sufficient layers to meet the requirements for the standard track finding algorithm.

The distribution for the number of hits associated with a reconstructed track is shown in Figure 3.7. The distribution has a peak at 10 hits, corresponding to tracks that fully traverse the detector. Most tracks have more hits that the 6 – 7 required by the standard track finding algorithm, but ~15% of the tracks have only 6 – 7 hits and are potentially at risk for not being reconstructed if one of the hit layers is missing.

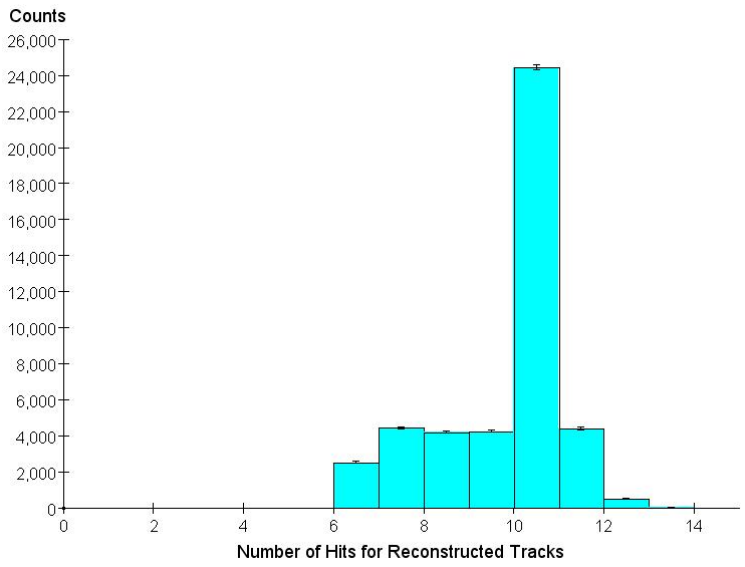

Figure 3.7 Number of hits associated with reconstructed tracks using the standard track finding algorithm with all tracker layers present.

In Figure 3.8, we show the track reconstruction efficiency for tracks reconstructed where the innermost vertex detector layer is missing (no VB0). We also show the efficiency when all layers are present for comparison. Both plots are constructed using identical efficiency "denominators" by selecting those tracks that are deemed "findable" with all layers present (see the LOI for a more detailed description of the criteria for a track being findable). Thus, the differences in this plot are entirely due to differences in the efficiency "numerator", namely the number of findable tracks that are reconstructed. A substantial loss in efficiency is observed at low transverse momentum for the case of a missing vertex detector layer, but for transverse momenta above ~0.5 GeV the differences are negligible. Similar results are obtained for the cases where the outermost vertex detector layer is missing (no VB4) and where the innermost tracker layer is missing (no TB0).

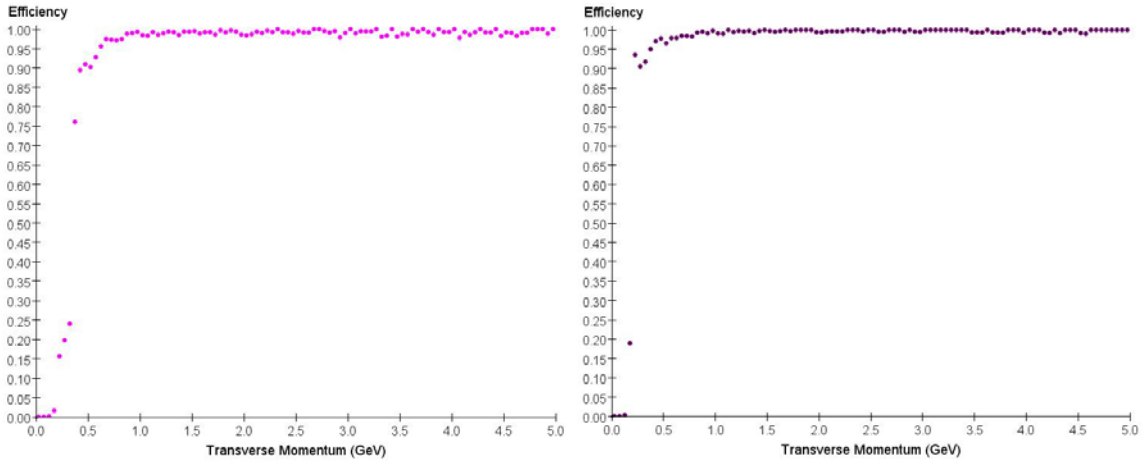

Figure 3.8 Track reconstruction efficiency with a missing inner barrel layer of the vertex detector (no VB0 - left) and with all layers present (All - right).

In Figure 3.9, we show the same plots for the case of missing the outermost tracker barrel layer (no TB4). Tracks that make it to the outer tracker layer will generally have 9 hits even without the outer tracker layer, which is more than adequate for track reconstruction in SiD. The loss in tracking efficiency from missing this layer is negligible.

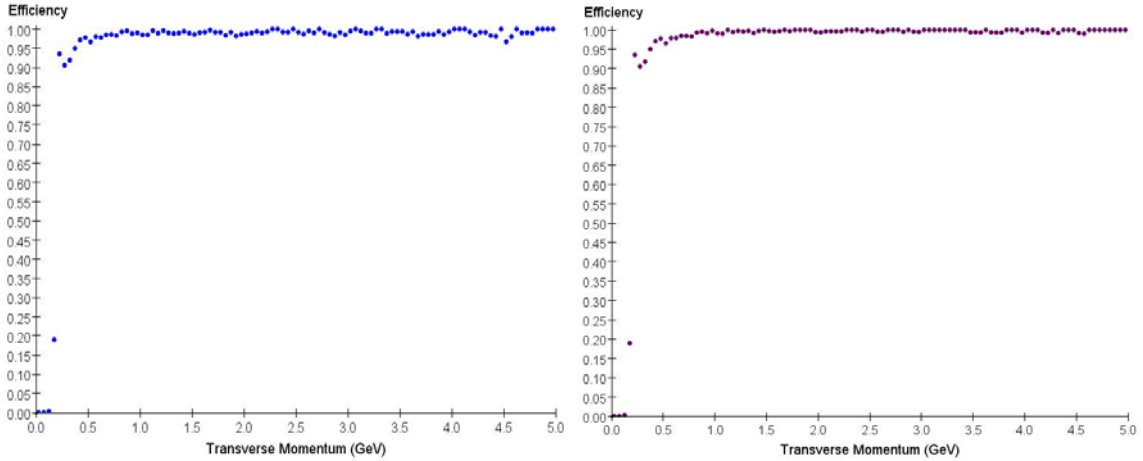

Figure 3.9 Track reconstruction efficiency with a missing outer barrel layer of the tracker (no TB4 - left) and with all layers present (All - right).

We have also measured the fake rate when a layer is missing. Fake tracks are identified as those having less than half their hits associated with a single Monte Carlo particle. In all cases, the fake rate remains small. The results for track reconstruction efficiency and fake rate for the cases studied are summarized in Table 3.1. Note that the loss in efficiency is essentially entirely at low momentum, so the fact that many tracks in $e^+e^- \to t\bar{t}$ events are soft translates into sizable losses in the average relative efficiency quoted.

Table 3.1 Track reconstruction efficiency and fake rate for the missing layer cases studied. The track reconstruction efficiency is normalized to the efficiency when all layers are present (All).

	All	No VB0	No VB4	No TB0	No TB4
Rel. Eff.	100%	(92.4±0.1)%	(93.8±0.1)%	(92.5±0.1)%	(99.3±0.1)%
Fake rate	(0.15±0.02)%	(0.09±0.02)%	(0.12±0.02)%	(0.03±0.01)%	(0.10±0.02)%

The results of these efficiency measurements are consistent with our expectations. The current tracking algorithm utilizes hits in all vertex detector barrel layers and the innermost tracker layer to find low momentum tracks that curl up before reaching the second tracking layer. Thus, missing one of these layers greatly reduces the track reconstruction efficiency at low momentum. It should be emphasized that all results are obtained with an algorithm that has not been optimized in any way. In principle, much of this inefficiency could be recovered with a more sophisticated track reconstruction algorithm that picked up additional hits for curling tracks. Since low momentum tracks will generally pass through the tracker endcap disks and proceed into the endcap EMCAL, endcap calorimeter assisted tracking will also recover many of the lost low momentum tracks. On the other hand, high momentum tracks cross most or all layers, and the loss of an outer layer has little effect on the track finding efficiency in the standard tracking algorithm. Note that the calorimeter assisted tracking algorithm relies heavily on the outermost tracking layer, so the loss of this layer would not be without consequences.

Q2: Give the efficiency and the fake track fraction in a jet environment with full background simulation.

The SiD detector concept takes advantage of the fast charge collection in silicon to minimize the impact of beam backgrounds. The silicon strip detectors in the outer tracker "time stamp" the beam crossing they originate from, providing single bunch time tagging. While the SiD vertex detector technology selection has not yet been made, we currently favor technologies that will also provide the ability to time stamp vertex detector hits with the beam crossing. Thus, we anticipate that the SiD tracker will be sensitive only to backgrounds from the same beam crossing as the physics event.

To study the impact of backgrounds, we compare the tracking performance for a physics sample with and without backgrounds. The physics sample used in this study is the same as for the LOI, namely 1000 $e^+e^- \to t\bar{t}$ events at $\sqrt{s} = 500$ GeV. For the sample with backgrounds, the beam-beam backgrounds expected for one beam crossing are added to the physics sample before digitization and reconstruction. The beam-beam background is derived from Guinea Pig simulations of the nominal ILC beam parameters, including the effect of beamstrahlung. Both samples are processed through the same simulation and reconstruction packages used in the LOI. To minimize differences due to statistical fluctuations, the exact same physics sample is used for both the with-background and without-background cases.

Table 3.2 shows the breakdown of contributions to the track finding efficiency. We find a substantial increase in the number of tracks failing the p_T cut. This is expected due to the large number of very low p_T tracks in the background sample. There is also a ~0.7% increase in the number of tracks found due to the presence of real charged tracks in the background sample that pass all tracking requirements. Except for these differences, the track finding efficiency is essentially unchanged with the addition of backgrounds. In particular, the track reconstruction efficiency for "findable" tracks is 99% independent of whether backgrounds are included or not.

Table 3.2 Track Finding Efficiency with and without backgrounds.

Selection	$t\bar{t}$ with Background		$t\bar{t}$ without Background	
	Count	Efficiency	Count	Efficiency
All Tracks	188209	-	51871	-
$p_T \geq 0.2$ GeV	48744	(25.90 ± 0.10)%	48472	(93.45 ± 0.11)%
Nhit ≥ 6	44265	(90.81 ± 0.13)%	43997	(90.77 ± 0.13)%
Seed Hits Present	44162	(99.77 ± 0.02)%	43894	(99.77 ± 0.02)%
Confirm Hit Present	44145	(99.96 ± 0.01)%	43877	(99.96 ± 0.01)%
$\|d_0\| \leq 1$ cm	44069	(99.83 ± 0.02)%	43801	(99.83 ± 0.02)%
$\|z_0\| \leq 1$ cm	43946	(99.72 ± 0.03)%	43261	(99.72 ± 0.03)%
Track Reconstruction	43518	(99.03 ± 0.05)%	43261	(99.05 ± 0.05)%

We have also examined the fake track rate in these samples. Fake tracks are identified as those having less than half their hits associated with a single Monte Carlo particle. The fake rate in the sample with background is found to be 0.006% higher than in the sample without background (0.064% vs 0.058%).

In conclusion, we find that the expected level of background hits has a negligible impact on the SiD track finding efficiency and fake rate. Using the SiD standard track finding algorithm, we observe a tracking efficiency of 99% for findable tracks with a fake track rate of 0.6% for top pair production, independent of whether or not background hits are included in the simulation.

C. References

[1] H.Yang, J.Deibel, S.Nyberg and K.Riles, "High-precision Absolute Distance Measurement using Frequency Scanned Interferometry", App. Opt. **44**, 3937 (2005).

[2] H.Yang and K.Riles, "High-precision Absolute Distance Measurement using Dual-Laser Frequency Scanned Interferometry Under Realistic Conditions", Nuc. Inst. and Meth. **A575**, 395 (2007).

[3] Tim Barklow, "Physics Data for Detector Calibration at Ecm = 91 & 500 GeV," MDI Session, June 12, 2006, LCSW06. See http://indico.cern.ch/materialDisplay.py?contribId=21&sessionId=11&materialId=slides&confId=568

IV. Answers to Questions about Benchmarking

A. IDAG Questions about Benchmarking

1. Repeat the recoil analysis with Z -> $\mu^+\mu^-$, e^+e^-, including the corrected ISR spectrum, and simulation of beam-background hits.
2. Z(e^+e^-)H inclusive: show the result of the analysis with and without the calorimeter
3. Calibrate the template analysis for mass resolution in t-tbar and neutralino/chargino channels: study the robustness of the method by addingmore comparison tables

B. Generation and Processing of Data to Answer Benchmarking Question

We preface our answers to the benchmarking questions with a brief discussion of the event generation, detector response simulation and reconstruction which was carried out to answer the questions above. Three aspects of this process are covered in turn, Event Generation, Detector Simulation, and Event Reconstruction, followed by a brief summary and acknowledgements. Answers to the IDAG questions above appear in Sections C, D, and E which follow this section.

B.1 Event Generation

B.1.1 $Z \to \mu^+\mu^-, e^+e^-$ Recoil Analysis

B.1.1.1 Beam Spectra

The luminosity spectra for the electron and positron beams were generated using the guineapig event generator. In the generation of the spectra for the 250GeV center-of-mass events for the LOI, the switch controlling whether initial state radiation (ISR) was simulated was inadvertently left on. Since the physics event generation software also included ISR, this was double-counted, leading to an overestimate of the radiation. The resulting physics distributions were dominated by this input spectrum, masking differences in the intrinsic detector performance. After much discussion with the author of guineapig and other involved parties, a corrected version of the control parameters was developed and this was used to generate the correct spectra. At the same time, the beam energy spread was also corrected (0.18% for e^+, 0.28% for e^-).

B.1.1.2 e^+e^-h and $\mu^+\mu^-h$ Signal Samples

Events with a l^+l^-h final state (with $l = e, \mu$), were generated at five discrete higgs masses, 119.25,119.7,120.0,120.3 and 120.75 GeV. Events were generated with 100% polarization for the e^+ and e^- beams and samples representing the expected ILC conditions of $80\% e^-$ and $30\% e^+$ polarization were generated in both the LR and RL combinations. Roughly half a million events were generated for each lepton species at each mass and polarization state. Including additional samples generated to understand systematics, over 12 million signal events were generated. The events were weighted to represent an integrated luminosity of $250\, fb^{-1}$. In addition to these large-statistics samples, which were used to derive the shape of the recoil mass distribution, ten discrete samples composed of unit-weight events representing independent exposures of $250\, fb^{-1}$ were generated. These events were analyzed, both with and without the addition of beam backgrounds (described later) to provide the expected final mass measurement.

B.1.1.3 Physics Backgrounds

In contrast to the LOI physics benchmarking exercise, where all relevant Standard Model physics backgrounds were generated and mixed to create data files which replicated what a real experiment would see, the backgrounds for this exercise were handled discretely. Samples were generated in eight distinct categories, weighted to represent an integrated luminosity of $250\, fb^{-1}$ and handled separately. Most background events will have the generator level cuts:

$$60. < M(l^+l^-) < 115.00$$

$$60. < E(l^+l^-) < 144.25$$

where $l = e, \mu$. In cases where a τ is in the final state, or when there is an ambiguity regarding which lepton pair comes from the Z, there are no such cuts.

- zz

  This category represents primarily the ZZ^* contribution. 4.70 million events were generated for the LR, and 3.76 million events were generated for the RL polarization configuration.
- ww

  This category represents primarily the WW and ZZ contribution. 9.82 million events were generated for the LR, and 2.45 million events were generated for the RL polarization configuration.
- lle3e3

  This category represents the $e^+e^-\tau^+\tau^-$ and $\mu^+\mu^-\tau^+\tau^-$ contribution. 3.30 million events were generated for each of the LR and RL polarization configurations.
- e1n1n3

  This category represents the $\tau^+\tau^-$ process where the τ is forced to decay to the $e\nu_e\nu_\tau$ final state, and the WW process, where one W decays directly to $e\nu_e$ and the

other decays to $\tau\nu_\tau$ with the τ subsequently decaying to $e\nu_e\nu_\tau$. 1.04 million events were generated for each of the LR and RL polarization configurations.

- e2n2n3

  This category represents the $\tau^+\tau^-$ process where the τ is forced to decay to the $\mu\nu_\mu\nu_\tau$ final state, and the WW process, where one W decays directly to $\mu\nu_\mu$ and the other decays to $\tau\nu_\tau$ with the τ subsequently decaying to $\mu\nu_\mu\nu_\tau$. 1.00 million events were generated for each of the LR and RL polarization configurations.

- e1e1

  This category represents the Bhabha scattering process. 3.26 million events were generated for the LR, and 2.79 million events were generated for the RL polarization configuration.

- e2e2

  This category represents the $\mu^+\mu^-$ final state process. 3.53 million events were generated for the LR, and 2.46 million events were generated for the RL polarization configuration.

- e1a

  This category represents the $e\gamma \to eee$ final state process. 5.35 million events were generated for each of the LR and RL polarization configurations.

B.1.1.4 Beam Backgrounds

Three categories of background arising from beam-beam interactions were considered: direct pair production, $\gamma\gamma \to hadrons$ and $\gamma\gamma \to \mu^+\mu^-$. The detector response to these events was simulated and later overlaid on the higgs recoil signal events at the detector hit level before being processed through the reconstruction. In each event, the e^+e^- pairs arising from one bunch-crossing were overlaid on each signal event. Events for the $\gamma\gamma$ processes were drawn according to a Poisson distribution representing the mean number of events expected per beam crossing, with a luminosity of $5.9855\times10^{-7}\,pb^{-1}$ per bunch.

- Guineapig Pairs

  Due to the very large numbers of e^+e^- pairs produced in each beam crossing, and the large amount of CPU time required to process them, events were not regenerated at 250GeV. Instead, events which had been generated and used in the background studies at 500GeV were overlaid on the higgs recoil signal events. We believe this represents a very conservative demonstration of the effect of the pairs backgrounds, and answers the question *"What happens if backgrounds are larger than expected?"*

- $\gamma\gamma \to hadrons$

  $216{,}965$ events of this type were generated, representing a $202190.9\,pb$ cross section. We expect then 0.121 events per bunch crossing.

- $\gamma\gamma \to \mu^+\mu^-$

  $433{,}931$ events of this type were generated, representing a $765060.9\,pb$ cross section. We expect then 0.458 events per bunch crossing.

B.1.2 t-tbar Mass Analysis

An additional sample of events was generated with a top quark mass of 174.5GeV to calibrate the template analysis. 780 thousand events were generated for the LR, and 361 thousand events were generated for the RL polarization configuration.

B.1.3 Neutralino / Chargino Analysis

Three additional SUSY event samples were generated with the gaugino masses offset by -0.5 GeV, for a total of 3.8 million events.

B.2 Detector Simulation

The detector response to these events was modeled using the Geant4-based full detector simulation program slic using the sid02 detector description, identically to the procedures described in the LOI. The simulation was conducted at a number of sites, utilizing the SLAC lsf batch farm, the FermiGrid cluster, as well as the LCG and OSG Grids. The event samples were normally split into files containing 1000 events each; this kept the files to a reasonable size and also allowed them to be run within the batch queue CPU time limits. The following table summarizes the location, number of jobs run and average time per job (in hours) for the various event samples described above.

Channel	Location	#jobs	Hours/job
llh	SLAC	12236	7.96
e1a	SLAC	9949	11.91
e1e1	SLAC	6050	7.30
e1n1n3	SLAC	2075	3.64
e2e2	SLAC	5994	2.42
e2n2n3	SLAC	1990	1.07
lle3e3	SLAC	9186	10.30
	gridpp.rl.ac.uk	1100	10.69
	desy.de	1087	11.42
	gla.scotgrid.ac.uk	800	13.80
ww	FermiGrid	12277	4.19
zz	SLAC	6754	14.11
	in2p3.fr	1556	11.35
	desy.de	705	11.40
	gridpp.rl.ac.uk	200	11.26
susy delMneu1 -0.5	gridpp.rl.ac.uk	727	5.17
	desy.de	700	5.55
susy delMneu2 -0.5	desy.de	1051	5.33
	gridpp.rl.ac.uk	201	8.76
susy delMch1 -0.5	desy.de	1035	5.38
	gridpp.rl.ac.uk	117	5.73
	in2p3.fr	83	5.80

sixfermion mtop174.5	desy.de	743	16.0
	gridpp.rl.ac.uk	400	17.27

B.3 Event Reconstruction

The events were reconstructed using the same production release software as described in the LOI. However, the events at 250GeV were not processed through the LCFIVertex package, since only electron and muon reconstruction were required for the analyses. The following table summarizes the location, number of jobs run and average time per job for the various event samples described above.

Channel	Location	#jobs	Hours/job
llh	SLAC	12236	4.98
e1a	SLAC	9130	0.32
e1e1	SLAC	5992	0.75
e1n1n3	SLAC	2074	0.37
e2e2	SLAC	5977	0.19
e2n2n3	SLAC	1990	0.11
lle3e3	SLAC	6460	0.51
ww	SLAC	12277	0.45
zz	SLAC	8803	0.90
susy delMneu1 -0.5	desy.de	998	2.75
	scotgrid.ac.uk	328	3.28
susy delMneu2 -0.5	scotgrid.ac.uk	799	3.47
	desy.de	453	2.78
susy delMch1 -0.5	desy.de	787	2.80
	scotgrid.ac.uk	435	3.10
	gridpp.rl.ac.uk	13	2.5
sixfermion mtop174.5	desy.de	1143	2.35

B.4 Summary

Successfully completing the exercise of responding to the questions the IDAG posed at the TILC09 meeting required the use of all available computing resources. The e^+ and e^- beam spectra were regenerated using the correct generator settings and also the asymmetric beam energy spreads. Over 68 million events were generated at 250GeV cms and over 4.9 million events at 500GeV cms. Essentially all of the events were successfully processed through both the detector response simulation and the event reconstruction, including the addition of beam-beam backgrounds for the higgs recoil signal samples. The missing files were accounted for by reweighting during the final analyses, but will be reprocessed in the fullness of time.

C. (Q1)Re-analysis of Higgs Recoil Mass and Cross Section with Corrected ISR Spectrum and Simulation of Beam Background Hits

1. Re-analysis of $e^+e^- \to ZH \to l^+l^-H$ with Corrected ISR Spectrum

The event generation, simulation and reconstruction for the $e^+e^- \rightarrow ZH \rightarrow l^+l^-H$ signal and the SM background with the corrected ISR spectrum is described above in Section B. The event selection criteria was left unchanged from described in the LoI. However, the electron identification has been improved relative to that described in the LOI as a result of studies made in response to IDAG's question to SiD about bremsstrahlung photon recovery in the e^+e^-H channel. The electron identification efficiency has been improved from 90% to 98% for electrons with energies above 20 GeV without any loss in purity.

The distributions for the Higgs signal after the analysis cuts are shown in Figure 4.1 assuming 250 fb^{-1} luminosity with the initial electron and positron polarization combination $e^-(80\%R)\,e^+(30\%L)$ and 0 fb^{-1} with the combination $e^-(80\%L)\,e^+(30\%R)$. These two polarization combinations will be referred to by their electron polarizations 80eR and 80eL. The e^+e^-H channel is shown with bremsstrahlung photon recovery included, since that procedure provides the largest signal sample and the smallest mass and cross section error. The height of the peaks have approximately doubled with respect to the distributions shown in LOI Figure 4.2.

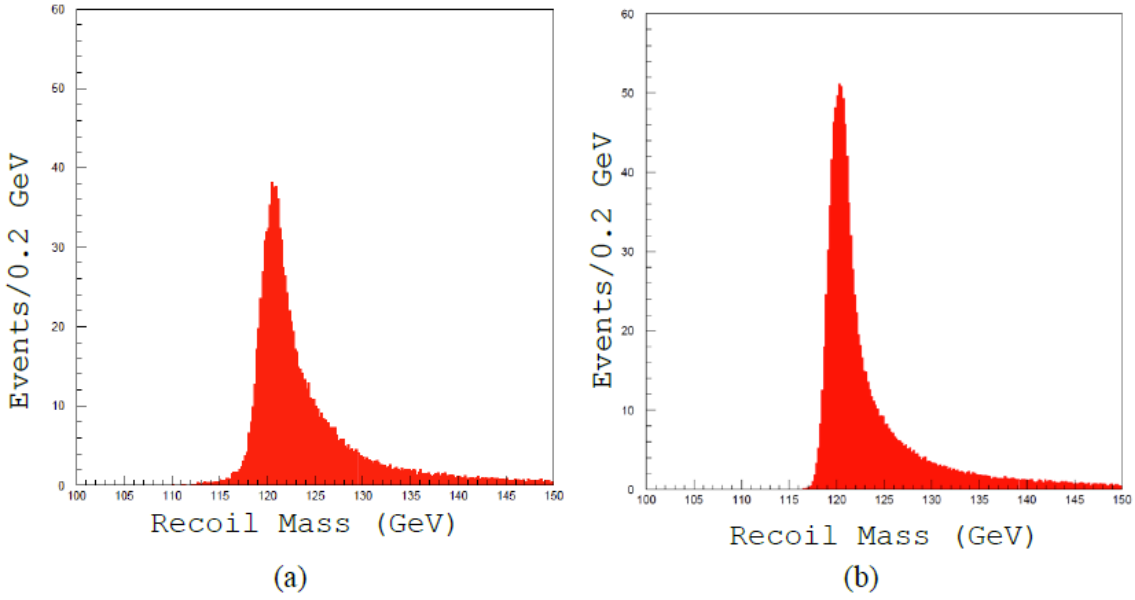

Figure 4.1 Recoil mass distributions following selection cuts for eeH (a) and μμH (b) assuming 250 fb^{-1} luminosity with 80 % eR initial state polarization. Background is not included. The electron reconstruction includes bremsstrahlung photon recovery.

A sample of 47 million fully simulated and reconstructed SM events were produced with the correct ISR spectrum as described in Section B above. This sample is composed of all the important SM background processes to $e^+e^- \to ZH \to l^+l^-H$. The distributions for the Higgs signals with background included are shown in Figure 4.2.

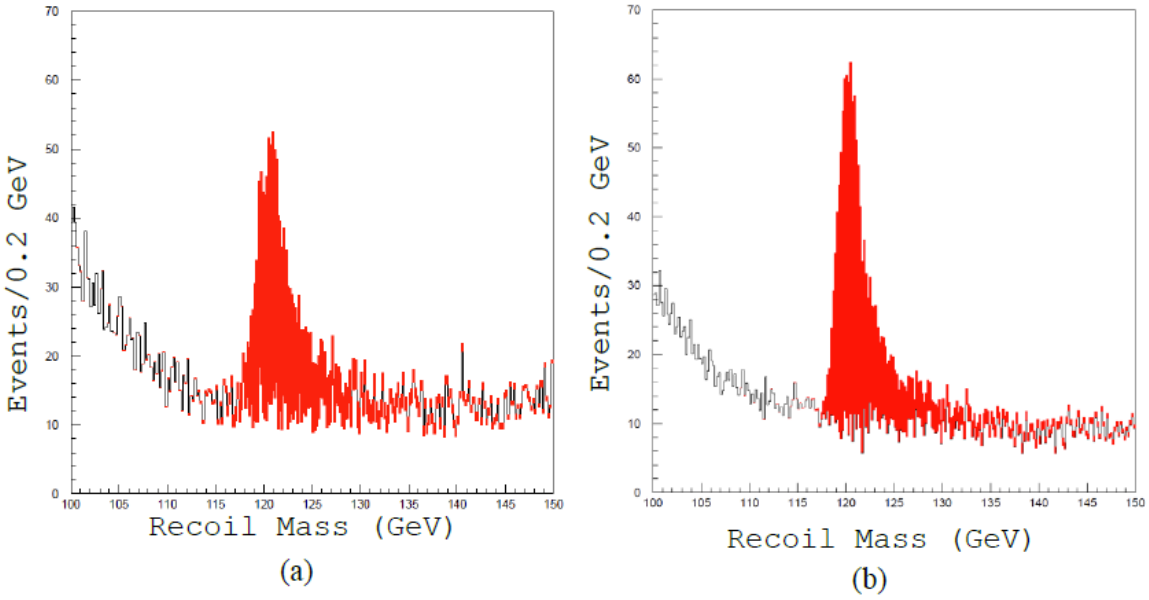

Figure 4.2 Recoil mass distributions following selection cuts for eeH (a) and μμH (b) assuming 250 fb^{-1} luminosity with 80% eR initial state polarization. The signal in red is added to the background in white. The electron reconstruction includes bremsstrahlung photon recovery.

Half of the large statistics signal samples with $M_H = 119.7$, 120.0, and 120.3 GeV, and all of the SM background samples were used as training samples to determine the parameters of linear least squares fit functions of the Higgs mass and cross section near $(M_H, \sigma_{ZH}) = (120\ GeV, \sigma_H^{SM})$. The statistical errors predicted from these least squares fit functions represent the total errors on the Higgs mass and cross section assuming that the background cross section can be calculated to arbitrary accuracy, that the luminosity spectrum and polarization can be perfectly measured, and that there are no detector systematic errors. In contrast to our studies for the LOI the training sample statistics are now large enough that the systematic error from Monte Carlo statistics can be neglected. The errors on the Higgs mass and cross section are summarized in Table 4. 1 assuming a recoil mass bin size of 0.2 GeV.

80eR lumi	80eL lumi	Mode	ΔM_H (GeV)	$\Delta\sigma_{ZH} / \sigma_{ZH}$
250 fb^{-1}	0 fb^{-1}	e^+e^-H	0.097	0.042
250 fb^{-1}	0 fb^{-1}	$\mu^+\mu^-H$	0.050	0.037
250 fb^{-1}	0 fb^{-1}	$e^+e^-H + \mu^+\mu^-H$	0.044	0.028
0 fb^{-1}	250 fb^{-1}	e^+e^-H	0.083	0.068
0 fb^{-1}	250 fb^{-1}	$\mu^+\mu^-H$	0.045	0.035
0 fb^{-1}	250 fb^{-1}	$e^+e^-H + \mu^+\mu^-H$	0.040	0.031

Table 4. 1 Summary of Higgs mass and ZH cross section errors for different channels and different luminosity assumptions.

The linear least squares fit functions obtained from the training samples were applied to independent 250 fb^{-1} luminosity test samples of signal and background. The signal for each test sample was independently generated, while the background for each recoil mass bin was randomly chosen according to a Poisson distribution with mean given by the bin content prediction from the large statistics SM background sample. The mean values and standard deviations for the distributions of fitted masses and cross sections are shown in Table 4. 2. The results are consistent with the errors shown in Table 4. 1.

# Samples	Mode	$< M_H\text{-}120> \pm \Delta M_H$ (GeV)	$< \frac{\sigma_{ZH}}{\sigma^0_{ZH}} - 1 > \pm \frac{\Delta\sigma_{ZH}}{\sigma^0_{ZH}}$
9	e^+e^-H	-0.028 ± 0.078	0.018 ± 0.035
62	$\mu^+\mu^-H$	-0.003 ± 0.042	-0.007 ± 0.040

Table 4. 2 Mean values and standard deviations for distributions of fitted masses and cross sections from collections of independent 250 fb^{-1} luminosity samples assuming 80eR initial state polarization.

2. Analysis of $e^+e^- \to ZH \to l^+l^-H$ including a Simulation of Beam Background Hits

The beam-beam background from $\gamma\gamma \to e^+e^-$, $\gamma\gamma \to \mu^+\mu^-$, and $\gamma\gamma \to hadrons$ was simulated and superimposed on several 250 fb^{-1} signal samples of $e^+e^- \to e^+e^-H$, as described in Section B above. The recoil mass selection criteria were applied to the reconstructed signal sample with and without the addition of beam background hits. In each case the presence of beam-beam background hits had very little effect on the recoil mass spectrum following selection cuts. A typical example is shown in Figure 4.3.

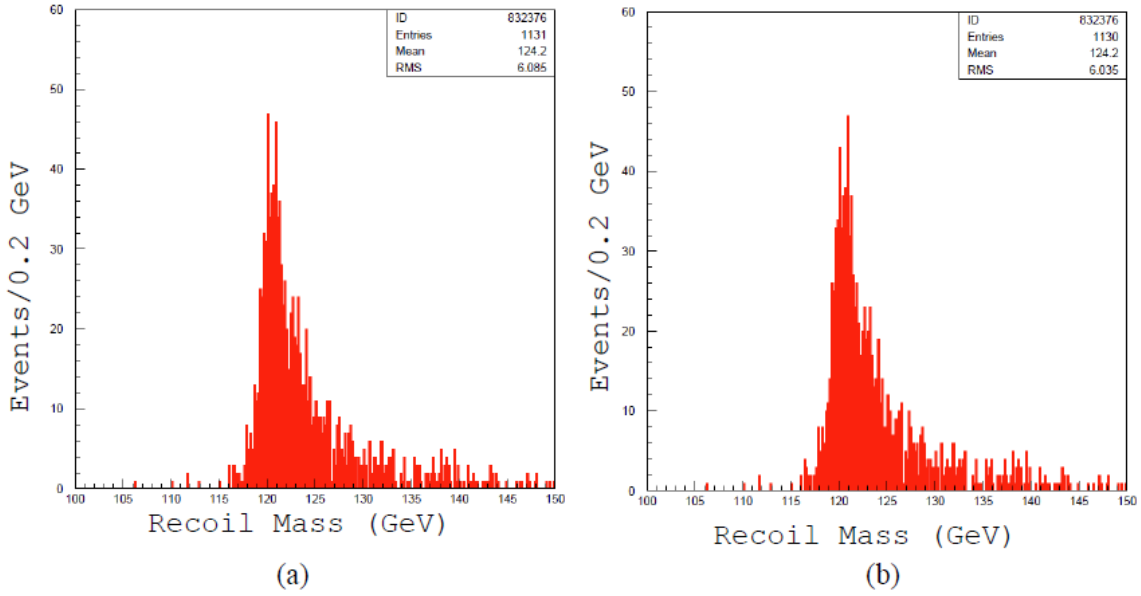

Figure 4.3 Recoil mass distributions following selection cuts for a 250 fb^{-1} eeH sample without beam-beam background hits superimposed (a) and with beam-beam background hits superimposed (b). The same eeH events are used in each case.

D. *(Q2)* Higgs Recoil Mass and Cross Section Analysis in the eeH Channel with and without Calorimeter Recovery of Bremsstrahlung Photons

Bremsstrahlung recovery is defined to be the association of photons with a track that has already been identified as an electron. The goal of the recovery is to improve the accuracy of the energy measurement of the electron that as undergone internal or external bremsstrahlung.

As mentioned above, this study employs a SiD electron identification algorithm different from that used in the LoI analysis, with improved performance. The old algorithm was improved by noting that electrons leave very little energy in the hadron calorimeter.

Electrons which failed the E/p cut, which may well have radiated bremsstrahlung photons, were recovered in this manner, and the electron identification efficiency was improved from 90% to 98% for electrons with energies greater than 20 GeV. Checks were made on SM processes ranging from tau pairs to top pairs to verify that the existing electron misidentification rate was not compromised.

Once electron identification was completed the invariant mass between an electron and each reconstructed photon was calculated. If this mass was less than 0.7 GeV the photon energy was added to the electron energy and the photon was dropped from the list of reconstructed photons. The recoil mass distribution with and without photon recovery is shown in Figure 4.4.

The improvement in the mass error and cross section error when bremsstrahlung photons are recovered is summarized in Table 4.3.

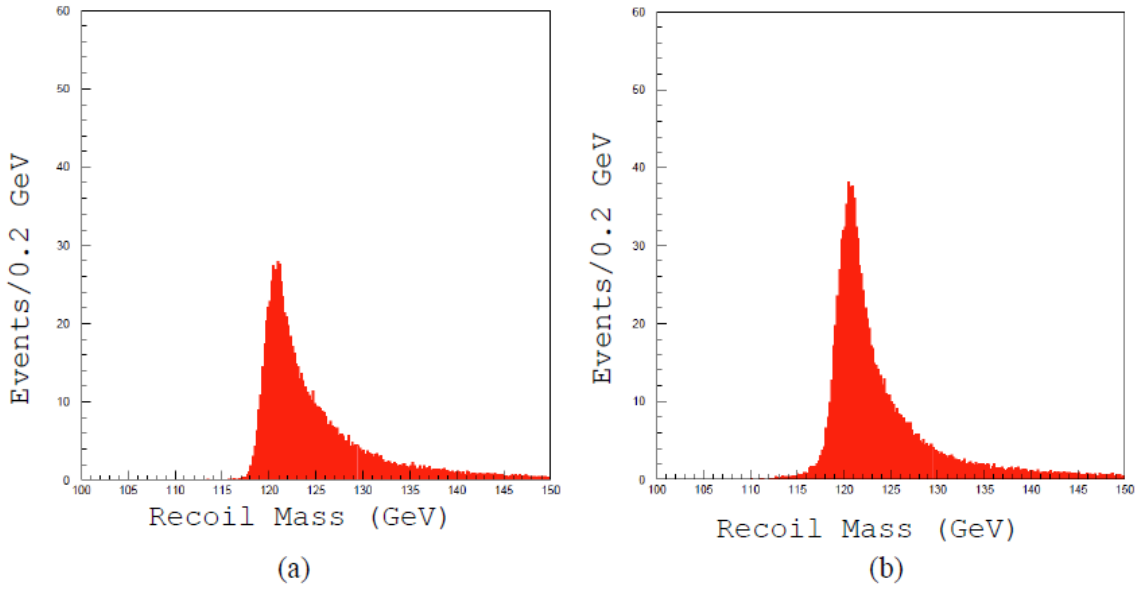

Figure 4.4 Recoil mass distributions for signal following selection cuts for (a) eeH without bremsstrahlung photon recovery and (b) with photon recovery assuming 250 fb^{-1} luminosity with 80eR initial state polarization.

80eR lumi	80eL lumi	Recover Brem γ ?	Mode	ΔM_H (GeV)	$\Delta\sigma_{ZH} / \sigma_{ZH}$ (%)
250 fb^{-1}	0 fb^{-1}	no	e^+e^-H	0.113	4.87
250 fb^{-1}	0 fb^{-1}	yes	e^+e^-H	0.097	4.15
0 fb^{-1}	250 fb^{-1}	no	e^+e^-H	0.102	8.36
0 fb^{-1}	250 fb^{-1}	yes	e^+e^-H	0.083	6.79

Table 4.3 Summary of Higgs mass and ZH cross section errors in the eeH channel with bremsstrahlung recovery turned off and on.

E. *(Q3)* Calibration of the template analysis for mass resolution in t-tbar and neutralino/chargino channels

The template analyses presented in the SiD LoI were limited by available time and resources and we benefited from additional time to perform extra checks. We used a toy MC model to investigate a number of scenarios and to study possible biases in the methods. Since the generation of templates using the full MC and reconstruction is very resource consuming we have added only several templates for the top and SUSY analyses. The analyses have been redone with an increased number of templates. We also repeated the SUSY analysis with modified assumptions to make them closer to the assumptions used by the ILD concept.

In general, we note that the template method had been extensively used by multiple experiments in HEP and is a well established technique. It allows a straightforward use of all available information and has a transparent statistical interpretation. The drawback of the method is that it is very resource intensive.

Template Method

The template method, briefly summarized below, was used to determine the top mass and chargino/neutralino masses. A Monte Carlo signal sample, 'data', is compared to several MC templates which have been generated using different values of a parameter which needs to be evaluated (e.g. top mass, chargino mass, etc.). The top mass and the W/Z energy are used as observables correspondingly in the top and SUSY analyses. The 'data' sample corresponds to 500 fb^{-1} but the templates typically have higher statistics.

One of the templates is generated with the same value of the parameter as the 'data' sample. The chi-square between these two distributions can be calculated as:

$$\chi^2 = \sum_{i=0}^{nbins} [y_{\{template\ 1,i\}} - y_{\{data,\ i\}} + \delta_i^2]/[\sigma^2_{\{template\ 1,i\}} + \sigma^2_{\{data,\ i\}} + \sigma^2_{\{SM,i\}}]$$

where $y_{\{...i\}}$ denotes the content of the ith bin of the histogram, and

δ_I is added as a Gaussian smearing of the central value of $y_{\{template\ 1,i\}} - y_{\{data,\ i\}}$

to take the SM background into account.
The calculated χ^2, normalized by the number of degrees of freedom (ndf), is expected to be close to one.

Similarly we can calculate the χ^2 for the 'data' using other template samples where the mass m_t is shifted by some amount. Then we can fit the χ^2 values assuming a parabolic dependence on mass. The parabola should be centered at m_t and ideally χ^2/ndf is equal to one at the minimum. The half width of the parabola where χ^2 is higher than its minimum by one gives the uncertainty of m_t. Figure 4.5 illustrates the method using two cases, the two point parabola fit (as in the LoI) and the five point parabola fit (as in toy MC below).

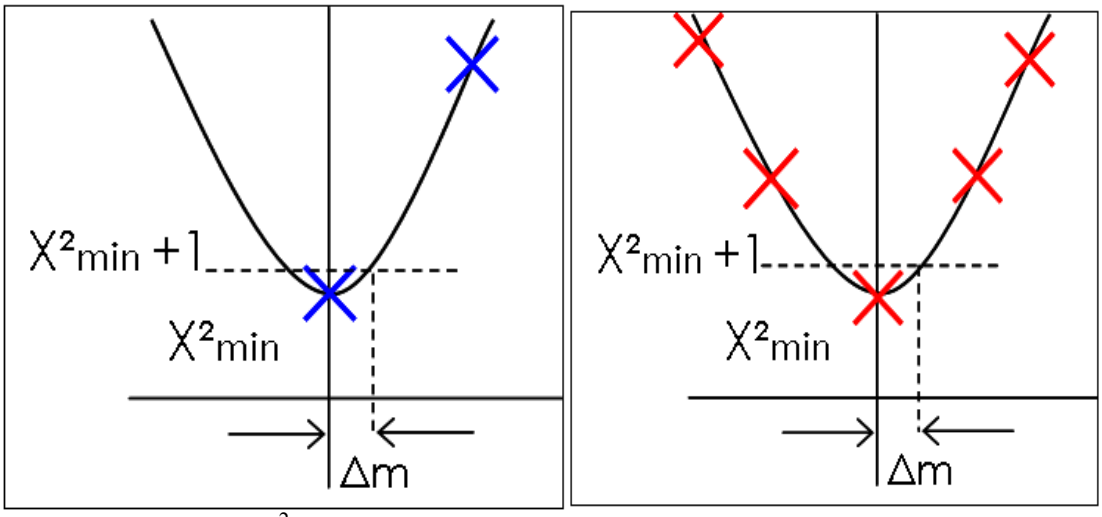

Figure 4.5 Fit of χ^2 parabola with two templates assumes that one of the points is at the minimum. Fit of χ^2 parabola with five templates requires no assumption on the location of minimum.

In our study described below we address two main points:

- We study possible biases of the template method using toy MC
- We redo the top and SUSY analyses using several additional points and assumptions

Toy Monte Carlo Studies

Toy MC is required since the time scale for completing these studies with full MC is prohibitive. We are convinced that the toy MC approach is adequate due to the purely statistical nature of the checks at this stage. The toy MC model used a Gaussian signal with mean at 80 and sigma of 10 with a variable level of flat background. The five template samples used the same distribution with means at 78, 79, 80, 81 and 82.

In this study we would like to show:

- The $\chi^2 + 1$ estimate gives the correct resolution
- Results obtained by fitting of χ^2 parabola using two templates and five templates are consistent.
- Our treatment of background as a Gaussian smearing is reasonable and the method works at various signal to background ratios.
- Results obtained by the template method and curve fitting method are consistent.

For each particular study we conducted a thousand toy experiments using five templates to fit the parabola and determined the minimum of the function in each case. The found minimum is an estimate of m_t in the corresponding experiment. The distribution of the minima is shown in Figure 4.6. The Gaussian fit of the distribution has sigma of 0.115 which is an estimate of the mass resolution. This is in good agreement with the resolution given by the χ^2 +1 estimate, 0.113. In this particular case the S/B ratio was equal to 10. The result does not depend on the m_t binning and has a weak dependence on the S/B ratio when it changes from 0 to 1.

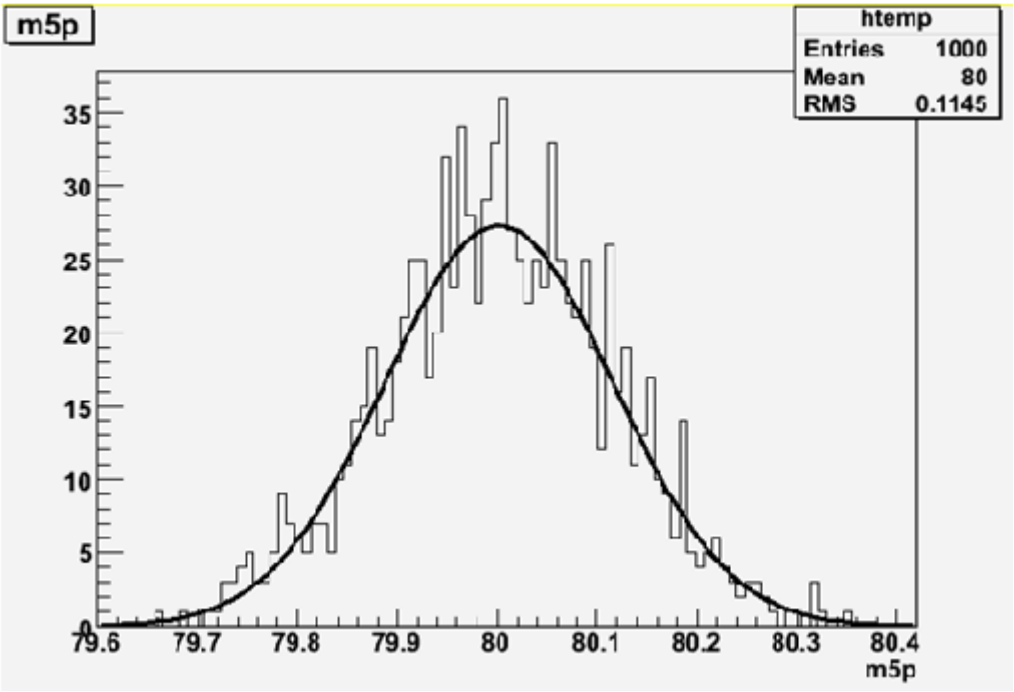

Figure 4.6 Distribution of the reconstructed masses in the five-point parabola fits**.**

Similar toy experiments were conducted to compare the template fits using two and five points. The resolution predicted by the χ^2 +1 estimate was found consistent in all the cases considered.

For the above studies the effect of the background was estimated using two approaches, first using the Gaussian smearing of the signal distribution and second by explicitly adding background events with flat distribution. The amount of the background was varied corresponding to the S/B variation from 0 to 1. In all cases the results were consistent.

We also compared results obtained by the template method and curve fitting method. The signal and background have been fit using the sum of a Gaussian and a constant leaving all parameters floating. The precision of the reconstructed mass determined from the fit was consistent with the precision in the template method.

Based on the above studies we conclude that the estimate of mass resolution for the top analysis and the estimate of the chargino/neutralino masses in the SUSY point5 analysis are reliable.

Additional Studies for the Top Analysis

In the LoI the top mass was determined using two techniques, curve fitting and templates. The precision for top mass quoted in the LoI is 53 and 38 MeV for the curve fitting and template methods, respectively. The latter used two top mass templates, 173.5 and 174 GeV.

In the post-LoI period the curve fitting result has been confirmed but for the template analysis a normalization mistake was identified which changed the result from 38 to 44 MeV. In addition the following studies have been performed to address the IDAG question on the template method.

A new mass point, 174.5 GeV, has been prepared using full MC, reconstruction and analysis chain, as for the previous templates. The parabola fit with the three templates gives the top mass resolution of 45 MeV, in agreement with the case of two templates. No dependence on the template binning was found. In all cases the estimated top mass was within one sigma from the generated value, 174 GeV. Figure 4.7 shows difference in two top mass templates with corresponding masses different by 0.5 GeV.

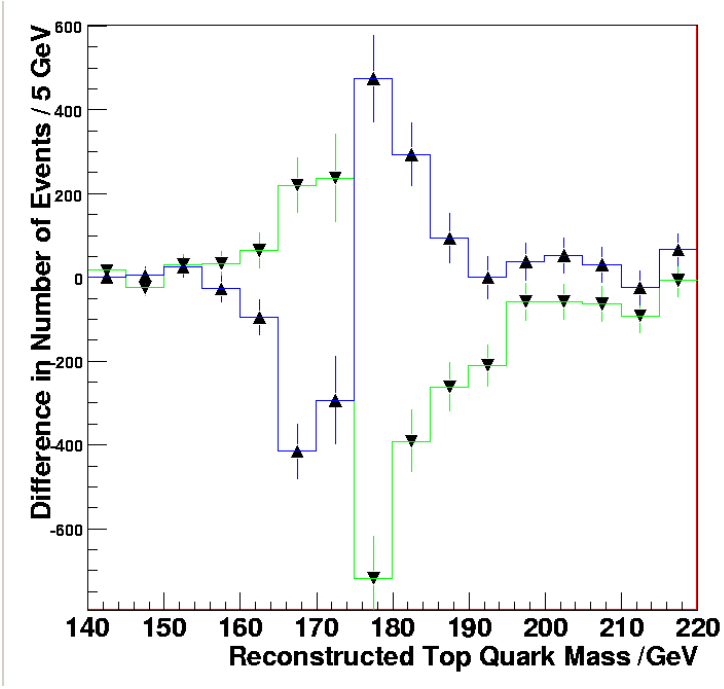

Figure 4.7 Difference of top mass templates with corresponding masses different by 0.5 GeV.

The difference between the 53 and 45 MeV resolution obtained with two different methods (curve fitting and templates) is explained by the fact that the template method implicitly uses the cross section information while the curve fitting does not. If the cross section dependence is removed from the templates by normalizing them to the same number of events then the mass resolution changes from 45 MeV to 49 MeV.

The remaining difference could be partly explained by different mass windows used for both methods in the LoI analysis. If the window which is used in the template method is narrowed to the same one as for the curve fitting the result changes from 49 MeV to 50 MeV.

We believe that this is a reasonable agreement (50 MeV versus 53 MeV) between the two methods. The remaining discrepancy might have been caused by lack of optimisation of the fitting procedure in the curve fitting method.

Additional Studies for the SUSY Analysis

Similarly to the top analysis three additional signal samples have been generated for the SUSY analysis to allow for three point parabola fits for the template method. All samples have been fully simulated, reconstructed and processed through the same selections procedures as described in the LoI. The results obtained under the same assumptions as in the LoI are fully consistent with the previous results.

Additional studies have been performed to modify the analysis assumptions removing the cross section information from consideration. To achieve this, different templates have been normalized to the same number of events so only the shape information is used for the mass determination. Figure 4. 8 a and b show the difference of the normalized mass templates with corresponding masses different by 0.5 GeV. The difference in shapes is quite obvious and manifests itself not only on the kinematic edge of the distribution.

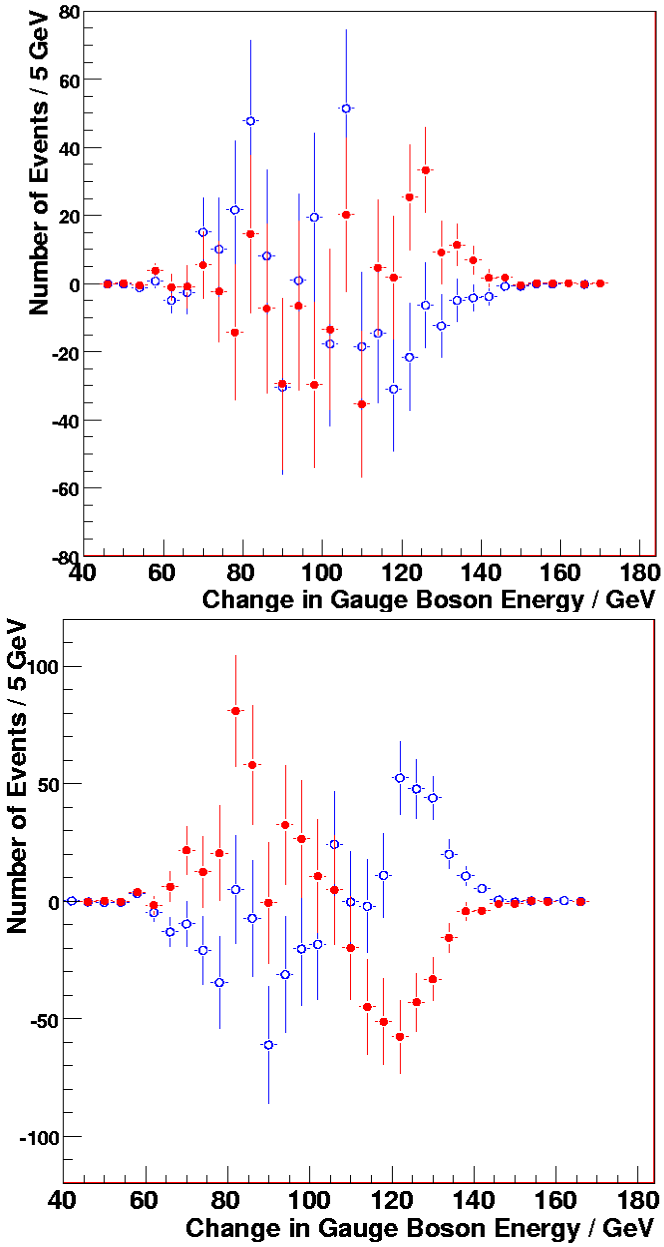

Figure 4. 8 a (top) Difference of templates with corresponding chargino masses different by 0.5 GeV; 4.8 b(Bottom) Difference of templates with corresponding first neutralino masses different by 0.5 GeV.

The mass uncertainties obtained with the new assumptions are 450, 490 and 160 MeV respectively for the chargino, second neutralino and first neutralino masses. These results have been obtained for the three point parabola fit. The results obtained with the two point parabola fit under the same assumptions are all consistent. Obviously the precision of the mass determination deteriorates when using only the shape information.

We are currently preparing new signal samples with a larger separation of masses to test the stability of the results.

V. Answers to Questions about MDI

A. Questions & Answers

Q1 - Numerics: Please, check the summary table (MDIsummary.xls) and correct any factual errors, or provide the missing numbers, in particular, for the items that follow –

The corrected spreadsheet is available on the same Web page as this document.

Q2 - Footprint: Please, indicate the envelope (or footprint) that the detector has to occupy during the maintenance period in the offline position.

See drawing Figure 5.3 (MDIidag3.pdf , see below)

Q3 - Shield blocks: Please, provide the rough size of additional shield blocks to use and their schematics (if they exist), when the detector is in the online position. The objects to consider include: pacmen, shield walls, others.

There is non need of additional shielding blocks since the detector is designed as "self shielded" versus the worst case of a full beam loss in the Qf1 region. The Pacmen are permanently integrated on the detector and on the cavern wall.
See drawing Figure 5.1 **MDIidag1**

Q4 - Platform and height: Please, indicate the assumed height of the platform beneath the detector, its size, its weight, and the assumed beamline height relative to the detector hall floor.

SiD does not use a platform, it moves on Hilman rollers over reinforced steel rails on the cavern floor. The motion is provide by strand jacks.

Q5 - Gross weight: Please, indicate the gross total sum of the weight of your detector system, including the barrel, endcaps, platforms (if any), and shield blocks.

Barrel,4500 t + Endcaps, 2x200 t + Pacmen, 2x170 t = 9840 t

Q6 - QD0: Please, indicate the Z locations of your QD0 (Zmin and Zmax) and their radius R to occupy.

SiD is optimized for an L* =3500 mm. The QD0 cryostat envelope is Zmin = 3236 mm, Zmax = 6886 mm. Radius is 190mm or less (current BNL design optimized for 4.5m L*).

Q7- Cryogenics: Please, indicate if your QD0 and the solenoids are to operate at 2K or 4K.

The SiD solenoid will be designed and operated at 4K. We assume that the QD0 will be designed by the BDS machine group and it will be operated at 2K.

Q8 - Push-pull motion:

a) Please, indicate the preferred method of push-pull motion mechanics that is currently under consideration.

b) Please, identify the hardware components (beamline elements, shield blocks, and utilities) that need to be disconnected/disassembled and reconnected/reassembled during your detector push/pull. Please, estimate how long this relocation / reassembly work will take.

c) Assuming that the accelerator (including QF1) is in a good alignment condition, how long would it take to complete your detector "push", and complete the alignment of the detector components? Explain how you will do this realignment; i.e. what kind of measurement and mover systems.

d) How long would it take to complete your detector "pull" and to make the interaction region and the BDS ready for the other detector?

e) During the upcoming Technical Design Phase, what type of resources do you plan to allocate for the conceptual and engineering work on MDI-related issues, and how you intend to operate them? Also, do you have any requests for assistance to the RD management or to the MDI group, in terms of resource sharing or in terms of interactions on technical matters?

a) SiD seats on four carts equipped with Hilman roller and hydraulic jacks. The carts move over a reinforced steel floor, pulled by strand jacks.

b) See Marty's talk given at TILC09 http://ilcagenda.linearcollider.org/getFile.py/access?contribId=30&sessionId=42&resId=0materialId=slides&confId=3154

c) The motion system considered for SiD is expected to provide an alignment precision within ±1 mm. An interferometer system is integrated on QD0 to monitor the final alignment on the beam, at the "pull" stage. During the beam operations, QD0 is quipped with integrated movers in feedback with BPMs, to achieve fine tuning and the correction of the optic alignment.

d) See Marty's talk given at TILC09 http://ilcagenda.linearcollider.org/getFile.py/access?contribId=30&sessionId=42&resId=0&materialId=slides&confId=3154

e) Assuming a serious effort to bring credible concepts to the technical design phase, SiD assumes that the level of engineering resources currently invested by the US and Europe will continue. Approximately 1 or >1 FTE/lab of ME/EE effort is currently being invested in SiD by BNL, FNAL and SLAC, respectively, and ~<1 FTE by the UK, France and Spain. We have a standing weekly engineering coordination meeting for SiD itself and are actively participating in the bilateral post-LOI efforts to engineer push-pull in a credible manner. We anticipate continued and valued collaboration with that part of the MDI group involved in the final doublet design, radiation shielding, fast feedback, vacuum, beamline instrumentation, IR layout and

other relevant MDI issues. We do NOT need or want to have an engineered IR solution delivered to us without our active collaboration in the design process.

MDI figures:

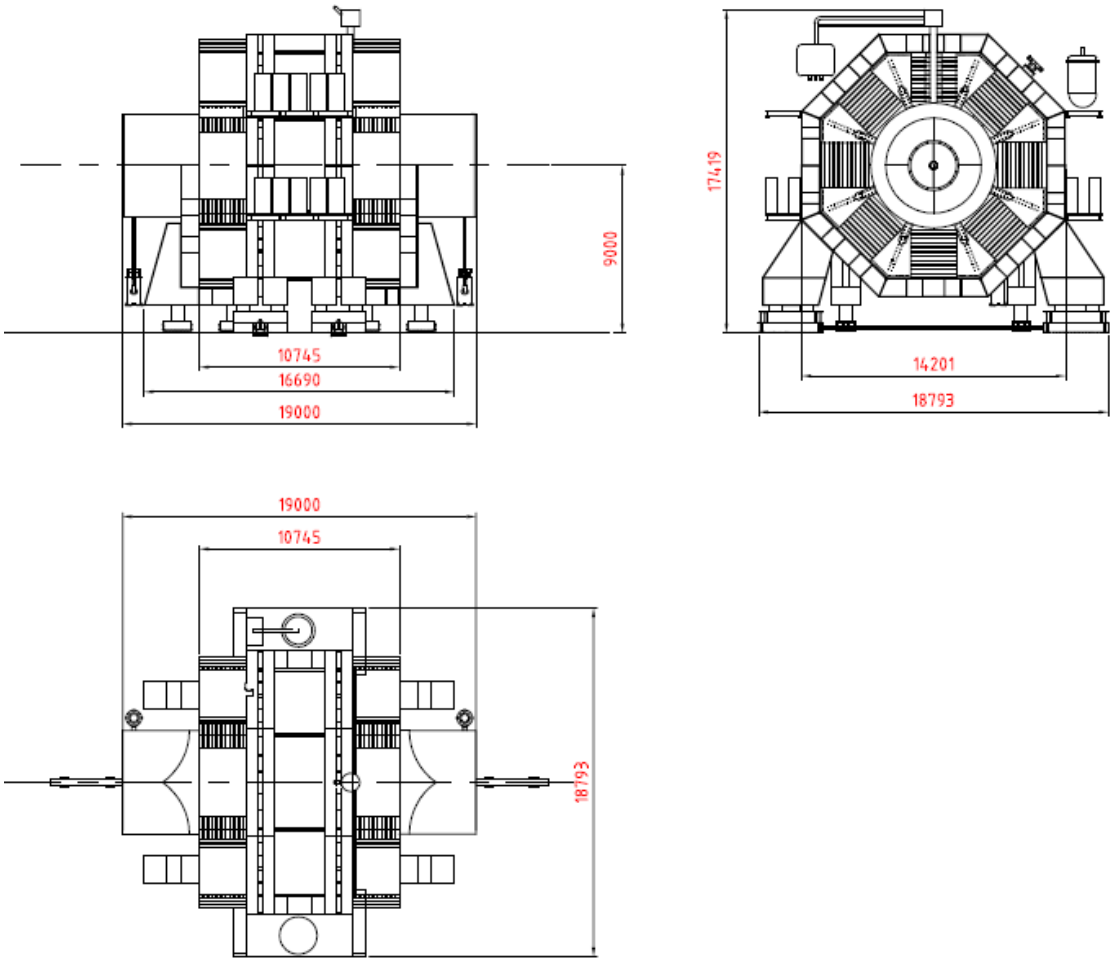

Figure 5.1 MDIidag1

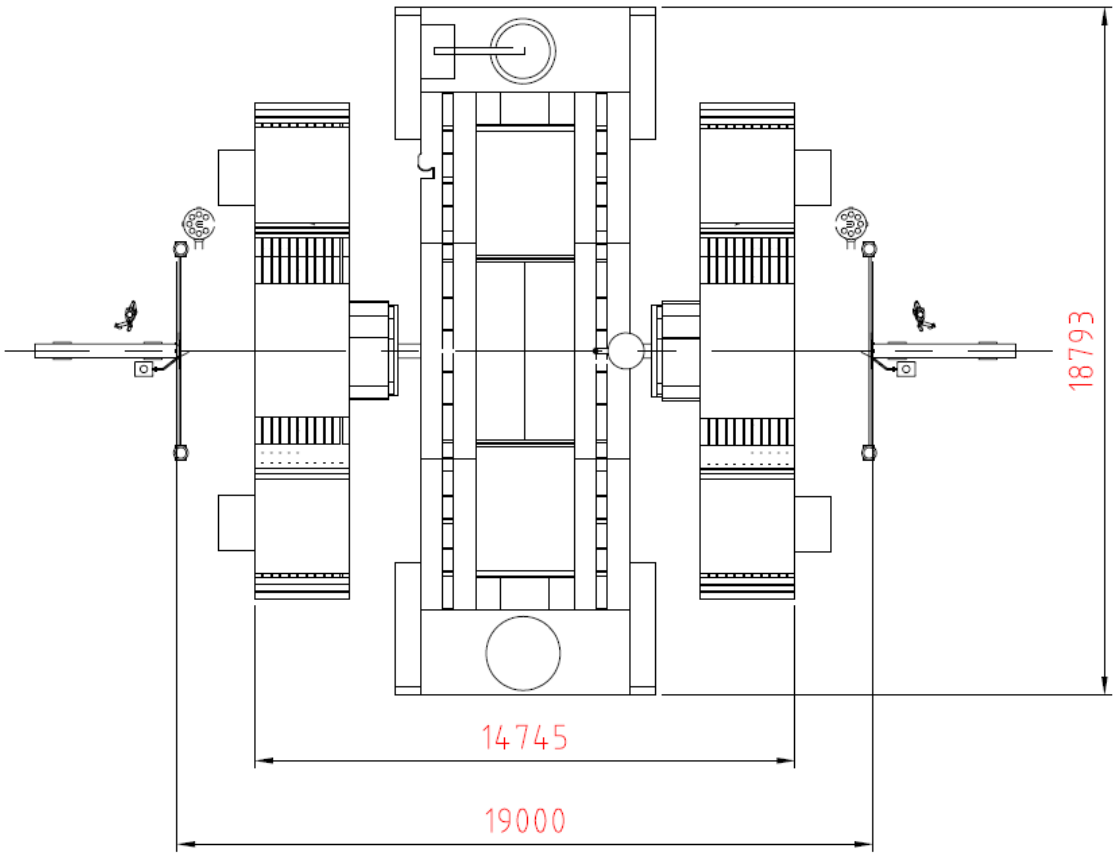

Figure 5.2 MDIidag2

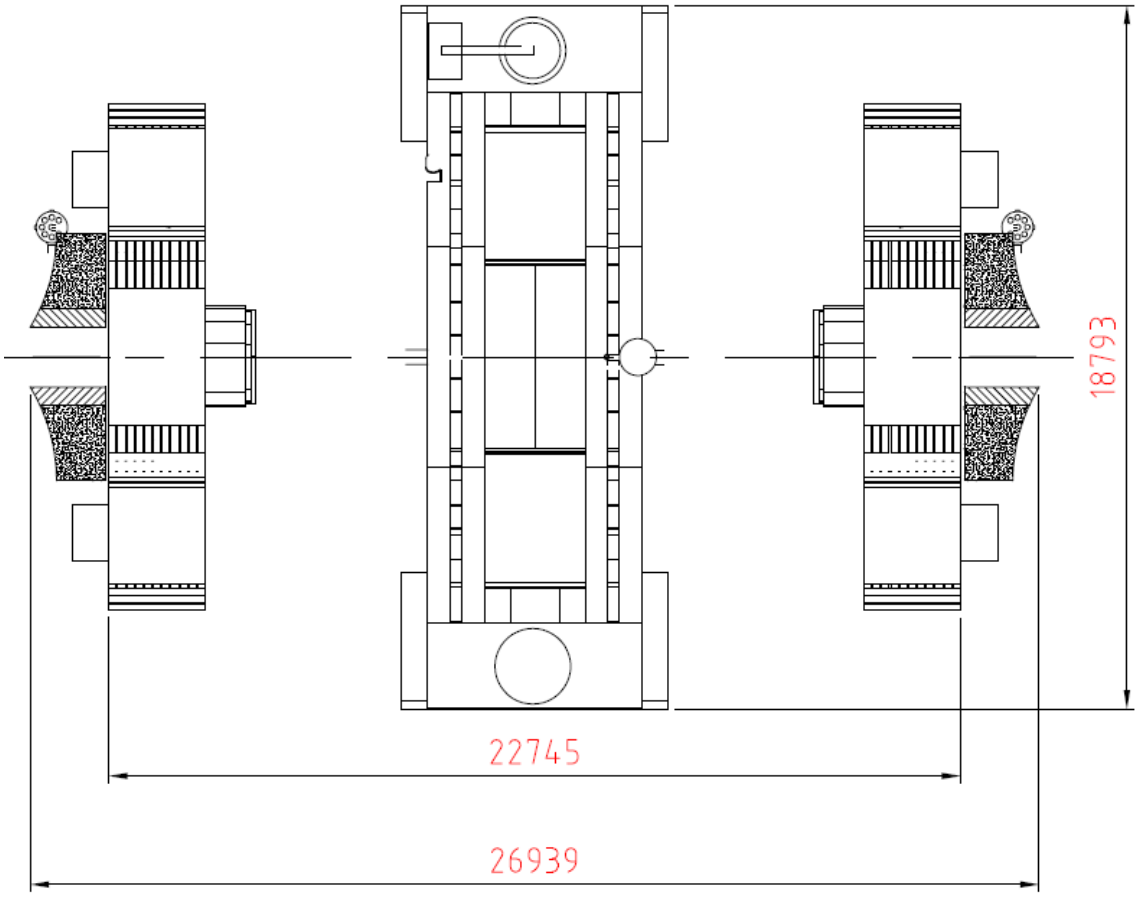

Figure 5.3 MDlidag3